Volume 1, No. 4 (2013)

International Review for Spatial Planning and Sustainable Development

SPSD Press from 2010

SPSD Press from 2010

International Review for Spatial Planning and Sustainable Development

For investigation regarding the impact of planning policy on spatial planning implementation, International Community of Spatial Planning and Sustainable Development (SPSD) seeks to learn from researchers in an integrated multidisciplinary platform that reflects a variety of perspectives—such as economic development, social equality, and ecological protection—with a view to achieving a sustainable urban form.

This international journal attempts to provide insights into the achievement of a sustainable urban form, through spatial planning and implementation; here, we focus on planning experiences at the levels of local cities and some metropolitan areas in the world, particularly in Asian countries. Submissions are expected from multidisciplinary viewpoints encompassing land-use patterns, housing development, transportation, green design, and agricultural and ecological systems.

Copyright©2010 SPSD Press. All rights reserved
IRSPSD INTERNATIONAL
ISSN 2187-3666 (Online)

International Review for Spatial Planning and Sustainable Development
https://www.jstage.jst.go.jp/browse/irspsd
http://spsdpress.jimdo.com/volumes/
http://dspace.lib.kanazawa-u.ac.jp/dspace/bulletin/irspsd

SPSD

International Review for Spatial Planning and Sustainable Development

Volume 1, No. 4, 2013

SPSD Press from 2010

Editorial Board

Editor-in-chief

Zhenjiang SHEN
School of Environmental Design
Kanazawa University, Kakuma Machi, Kanazawa City,
Japan, 920-1192
shenzhe@t.kanazawa-u.ac.jp; fcl.shen@gmail.com
Tel.0081-76-234-4650

ANDO, Ryosuke,	*Toyota Transportation Research Institute*
BALABAN, Osman	*Middle East Technical University*
BOQUET, Yves	*Université de Bourgogne*
DANG, Anrong	*Tsinghua University*
DRAGICEVIC, Suzana	*Simon Fraser University*
GAO, Xiaolu	*Chinese Academy of Sciences*
JIANG, Bin	*University of Gävle*
KAWAKAMI, Mitsuhiko	*Kanazawa University*
KINOSHITA, Takeshi	*Chiba University*
HUANG, Guangwei	*Sophia University*
LIN, Jen-jia	*Taiwan University*
LIU, Yan	*The University of Queensland*
MAO, Qizhi	*Tsinghua University*
MA, Yan	*Chinese Academy of Sciences*
MOON, Tae-Heon	*Gyeongsang National University*
NADIN, Vecent	*Delft University of Technology*
NEWELL, Josh	*University of Michigan*
OHGAI, Akira	*Toyohashi University of Technology*
OSARAGI, Toshihiro,	*TOKYO Institute of Technology*
PAI, Jen-te	*Chengchi University*
PENG, Kuang-hui	*Taipei University of Technology*
PENG, Xizhe	*Fudan University*
SUGIHARA, Kenichi	*Gifu keizai unveristy*
WIKANTIYOSO, Respati	*Universitas Merdeka Malang*
YAO, X. Angela	*University of Georgia*
YE, Kyorock	*LEARN*

Manager editor

LONG, Ying, Assoc. Prof. PhD, Beijing Institute of City Planning
Contact: longying1980@gmail.com

Editorial Secretary

Mr. LI, Yunfeng,
Contact: irspsd@gmail.com

Assistants

PINDO, Tutuko; LI, Xuefei;THANH, Nguyen; ZHANG, Yongping; LIU, Cuiling and LI, Miaoyi

International Review for Spatial Planning and Sustainable Development,
Volume 1 No. 4, 2013

Content

International review for spatial planning and sustainable development, Vol.1 No.4 (2013), 1-12
ISSN: 2187-3666 (online)
DOI: http://dx.doi.org/10.14246/irspsd.1.4_1

Copyright@SPSD Press from 2010, SPSD Press, Kanazawa

The Influence of Evapotranspiration by Urban Greenery on Thermal Environment in Urban Microclimate

Chih-Hong Huang[1*] and Pin-Yi Lin[1]
[1]*Gradeate Institute of Architecture and Urban Design, National Taipei University of Technology*
[*]*Corresponding Author, Email: huangch@ntut.edu.tw*
Received 1 Feberuary 2013; Accepted 19 July 2013

Key words: Urban heat Island, Evapotranspiration Effect, Green Planting, Computational Fluid Dynamics, Urban Microclimate, Urban Thermal Environment.

Abstract: The purpose of this research is to discuss the phenomena and temperature induced by the evapotranspiration from urban street greenery and pavement construction. We expect to achieve a good ventilation and temperature reduction with the improvement of planting and the pavement material. This research utilized Penman-Monteith equation to calculate the calorie needed for the evaporation of plant and realized the temperature reduction effectiveness by the evapotranspiration in the high temperature urban area via Computational Fluid Dynamics simulation. The results show that the planting has significant influence on the urban temperature reduction and the evapotranspiration of plant can ease off the urban high temperature situation. While under a windless condition, in compare with a windy environment which has better temperature reduction effect, the heat is difficult to dissipate due to the static status of the wind field. With regards to buildings, heat tends to accumulate at the windward and lee side of the building by eddy effect. For the future urban design code, the wind directing by plant and the ventilation of pedestrian wind field shall both being considered to alleviate the high temperature situation.

1. INTRODUCTION

With the process of urbanization, the tall dwelling buildings, business buildings and artificial pavement have gradually substitute the nature greenery and water area. Moreover, the air pollution caused by automobiles has made the heat coming from the solar radiation and artificial hear sources even more difficult to dissipate in the urban climate and worsens the urban thermal environment and reduces the human comfort feeling toward the environment.

In order to alleviate the urban thermal condition, scholars from many countries utilize the weather data, remote images, model simulation and site observation to probe into the research of heat island effect. Planting has been considered one of the most effective methods to improve the outdoor climate. There are abundant studies of urban microclimate indicate that the raise in "green coverage Ratio" could improve the urban temperature environment (Arnfield, 2003).

Previous Studies suggested that different planting models can reduce the urban temperature in a urban wind field and its arrangement, location,

evapotranspiration amount, solar radiation and the albedo of the surrounding pavement influence the temperature variation (Gromke et al., 2007; Lin et al., 2008; Fahmy et al., 2010).

The urban greening could efficiently reduce the load to the environment as well as having the function to modulate the urban microclimate, regulate the water and purify the air. Plants can absorb and reflect solar radiation to reduce the long wave radiation heat, and the shades generated by plants can block the direct sunlight to reduce the water dissipation from the air. The thermal environment becomes an important issue in urban design (Giridharana et al., 2007; Golany et al., 1996).

The urban microclimate effects seasonal outdoor thermal comfort a lot (Lin et al., 2011). It can lead to a rapid increase of energy consumption.

Lin et al. (2008) simulated and compared the urban temperature reduction effectiveness between bush, arbor and grass under the same surface area. By comparing grass with bush, the result showed an inapparent result in the improvement of human body thermal comfort by planting bushes around the buildings, which is due to the wind field speed reduction by the bushes and the sun position variation; while the grass has larger contact area which helps to remove the heat from the sun and improve the surrounding temperature. However, as to the average temperature, growing arbor has significant efficiency in improving the temperature of pedestrian wind field. Comparing with bush, arbor has shade effect due to its height which can generate a low temperature condition in the shadow area by blocking the direct sun light. Moreover, different vegetation patterns, arrangement and orientation around the building could result in different effect on human body thermal comfort.

This research utilized the CFD technique and explored the influence of temperature reduction variation by urban pavement and vegetation and its arrangement on urban wind field and temperature field. At last we proposed a few suggestions on the application of vegetation regarding the control of urban microclimate wind field in order to meet the urban eco-construction principle.

2. METHODOLOGY

This research had precisely simulated every kinds of eddy current in the street through the CFD environmental interference model and realized how each environmental factor affects on current change, temperature reduction and energy dissipation via different parameter settings.

2.1 Wind Field Theory

In order to simplify the complex mixed flow field theoretical model, this research assumed a steady, three-dimensional and uncompressible turbulence model for numerical simulation in the analysis process.

Since the space is under the same atmosphere condition, we can treat it as an isothermal condition and calculate the flow field velocity and pressure with the continuous equation and momentum equation. For the turbulence simulation, we introduced k-ε turbulence model to analyse the wind field status.

The standard k-ε model is established on the turbulent kinetic energy k equation basis with the introduction of a turbulent dissipation rate ε equation. The k-ε model was firstly proposed by Launder and Spalding in 1972 and soon became a primary tool for engineering flow field calculation. The equations mentioned above are shown below.

Continuous Equation:

$$\frac{\partial u_i}{\partial x_i} = 0. \qquad (1)$$

Momentum Equation:

$$\frac{\partial}{\partial t}(\rho u_i) + \frac{\partial(\rho u_i u_j)}{\partial x_j} = \rho g_i - \frac{\partial p}{\partial x_i} + \frac{\partial}{\partial x_j}\left[(\mu_{eff})\left(\frac{\partial u_i}{\partial x_j} + \frac{\partial u_j}{\partial x_i}\right)\right]. \qquad (2)$$

k-ε turbulence dual equation:

$$\frac{\partial \rho k}{\partial t} + \frac{\partial \rho u_i k}{\partial x_i} = \rho P - \rho\varepsilon + \frac{\partial}{\partial x_i}\left[\left(\mu + \frac{\mu_t}{\sigma_k}\right)\frac{\partial k}{\partial x_i}\right]. \qquad (3)$$

$$\frac{\partial \rho \varepsilon}{\partial t} + \frac{\partial \rho u_i \varepsilon}{\partial x_i} = C_{\varepsilon 1}\frac{\rho P \varepsilon}{k} - C_{\varepsilon 2}\frac{\rho \varepsilon^2}{k} + \frac{\partial}{\partial x_i}\left[\left(\mu + \frac{\mu_t}{\sigma_\varepsilon}\right)\frac{\partial \varepsilon}{\partial x_i}\right]. \qquad (4)$$

In the above equations, ui denotes the velocity vector at j direction, while p, ρ, μeff, m and gi represent pressure, density, effective viscosity coefficient (incl. both flow viscosity coefficient and turbulence viscosity coefficient, $\mu_{\text{eff}} = \mu_l + \mu_t$), material concentration mass fraction and gravity individually. In addition, μt= Cμ ρk2/ε, where k and ε denote the turbulence kinetic energy dissipation rate and turbulence kinetic energy generation rate individually. And the constants are set as Cμ=0.09, Cε1=1.44, Cε2=1.92, σk=1.0, σε=1.3, σl=1.0 and σt=1.0. The turbulence kinetic energy generation rate is represented by the following equation:

$$P = \frac{\mu_t}{\rho}\left(\frac{\partial u_j}{\partial x_i} + \frac{\partial u_i}{\partial x_j} - \frac{2}{3}\frac{\partial u_m}{\partial x_m}\delta_{ij}\right)\frac{\partial u_j}{\partial x_i} - \frac{2}{3}k\frac{\partial u_m}{\partial x_m}. \qquad (5)$$

The numerical method introduced in this research is SIMPLEC algorithm, which was used to derive the govern equation to further calculated the wind field distribution in the simulation space. The procedure is to integrate the original equation with the transient term discretized by one order Backward Difference and the convection term by First-Order Upwind Scheme to meet the steady numerical calculation demand. After the completion of finite volume difference equation, the pressure value was revised using SIMPLEC algorithm to derive the velocity field.

2.2 Thermal Conduction Theory

The thermal conduction does not rely on medium movement, but is a kinetic energy transmission mechanism through the rapid oscillation and collision of the molecule of high temperature (or high kinetic energy) zone to that of the low temperature zone. Such conductive heat transmission principle is called Fourier law. The thermal energy transmitted by temperature gradient is called the sensible heat. The sensible heat flux of a unit area is shown as,

$$H = -C_T\frac{\partial T}{\partial z} \qquad (6)$$

In the above equation, H denotes the sensible heat flux of the area (W m-2), C_T denotes the thermal conductivity (Wm-1K-1) and T denotes the temperature (°K). In the model, we defined the vegetation volume as polypore material and the heat flux as a constant and set the parameters on the volume boundary. For such convectional heat flux setting, we calculated the convection of the external

environment, which is the computational mesh system outside the area, but not only calculate the surface thermal energy. The equation for calculating the conductive wall is,

$$q_w = h_c(T_{ext} - T_w) \quad (7)$$

Where h_c is the external conductivity and T_{ext} is the external temperature.
In this research, we considered the pavement of different material and excluded the influence of other factors and set the surface condition as isothermal, i.e. a constant value. The equation is shown as,

$$q_w = -k\frac{T_c - T_w}{dx} \quad (8)$$

Where K denotes the conductivity of the fluid or the solid, T_c denotes the centre temperature and dx is the distance to the wall.

2.3 The calculation of vegetation evapotranspiration

The evapotranspiration is not only in relation to weather conditions, but also the water content in the soil, ground vegetation and the types or growing characteristics of vegetation. It is not always in proportion to the soil evapotranspiration. The water content of unit leaf area of the plant within a certain time is called the transpiration rate, and $g/cm^2/h$ is the unit often used.
The energy balance method is often used in many researches for computing the evapotranspiration of ground. We used the revised version of Penman equation - Penman-Monteith equation, to calculate the vegetation evapotranspiration, which uses the relations between aerodynamic resistance and the crop canopy resistance to substitute for the original wind speed function.
The Penman-Monteith Method was published by the International Committee of Irrigation and Drainage (ICID) in 1994, which was experimented the evapotranspiration on Lucerne and grass. The equation is as below (Allen et al., 1998).

$$EA = \frac{0.408(R_n - G) + r\frac{900}{T+273}u_2(e_s - e_a)}{\Delta + r(1 + 0.34u_2)} \quad (9)$$

Where EA is the evapotranspiration (mm/day); △ is the slope of vapor pressure curve (kpa/°C)' r is the psychrometric constant (kpa/°C); u_2 is the measured wind speed (m/sec) at 2 meter height; e_s-e_a is the saturation vapor pressure and the actual vapor pressure (kpa).
For the field application, the equation (9) requires the daily, weekly, every ten days or monthly data of air, temperature, psychroradiation and wind speed (Allen et al, 1998).

3. THE SETTING OF SIMULATION PARAMETERS

3.1 The setting of space parameters

This research focused on the discussion of urban external flow field. In addition to the discussion goal setting, we need to establish a simulated air field. Hence, the boundary conditions for the external space establishment of the global simulation are defined as 1) the area of 996m×1449m×200m; 2) the total mesh count is 794.025 and 3) the minimum mesh distance is 0.15m on the no-slip condition, in order to obtain a more precise computation. Regarding the wind direction in the inlet, we focused on the U direction which is perpendicular to

the X axis which is parallel to the building group. The inlet wind speed is set to the average wind speed of 1m/s and 5m/s referring to the ground friction (*Table 1.*), where the 1m/s is a hypothetically defined minimum speed for the minimum wind in the urban wind field in order to derive a steady state solution, which was treated as the contrast group of the heat convection and conduction in the urban wind field under the windless state.

Table 1. The reference table of the wind speed of different heights under an average wind speed of 1m/s and 5m/s

Height	0	1.5	3	5	10	15	25	50	70	100
T1	0	0.39	0.46	0.52	0.62	0.69	0.78	0.93	1.01	1.11
T5	0	1.94	2.30	2.62	3.11	3.44	3.91	4.65	5.06	5.53

Unit: Height (m); Wind speed (m/s)

3.2 The setting of ground parameters

3.2.1 The setting of building surface parameters

The area of the simulated construction base in this research is 36m×39m, which was divided into six zones of the same size with each zone an identical building of 10m×10m×20m volume on top of it. There is a backyard in each zone and to the east of the base are a 3m wide sidewalk and a 30m wide road, which has 10m wide greenery along the both sides. The surface material of the building is defined as reinforced concrete with the wall thickness of 0.155m and the heat conductivity of 3.78 W/m^{2}K. And the heat flux of the reinforced concrete wall is set to 0.61 W/m^{2}K, which was referred to the thermal comfort data of the building surroundings simulated by Jiang He and Akira Hoyano. Therefore, these data was arranged as the reference data and entered to CFD simulation software in this research. (Hang et al., 2010)

3.2.2 The setting of pavement related parameters

In the urban environment, the wind filed generates different friction force over different pavement materials and the heat absorption and release vary in different ground materials due to different levels of water content. We adopted the heat flux of different pavement measured by Hueimin Huang as the reference for this research and considered the heat flux of asphalt and grass pavement as the reference data for the simulation. The grass evapotranspiration was set to 6.35(mm/day) referring to the evapotranspiration of Saint Augustine Grass deduced by C. Tang, et al. in 2005 using Penman- Monteith method and calculated the required energy for the evapotranspiration as the input data for the simulation software.

3.2.3 The setting of vegetation and evapotranspiration

The setting of vegetation covers many complex factors. Therefore, we chose the common sidewalk tree in Taipei - Alstonia scholaris, as the simulation basis and set the height of 10m with branches of 3m, the pore size of 0.6 and the permeability of 0.00009 to calculate the evapotranspiration of the simulated greenery surface area deduced from the data measured by Wang et al. (2005). Since the evapotranspiration of vegetation is impacted by the factors such as sunlight and shading, we assumed noon time in this research to exclude the vegetation shading and sunlight issues (Bittelli et al., 2008). The relative parameters for the research model are arranged as *Table 2.*

3.3 The configuration of the simulation model

This research explored the change of wind field and temperature field by different pavement under a windless and windy condition in the urban environment (Baskaran et al., 1996). Hence, we defined the asphalt pavement as the basic condition and explored the scenarios as follows: grass pavement only, grass pavement with street greening (abbreviated as growing one row of trees), grass pavement, street greening and building backyard greening (abbreviated as growing two rows of tree). We calculated the temperature difference and the energy dissipation under various conditions and discussed the occurrence of evapotranspiration. There are 14 models and the simulation illustration of different pavements is shown in *Fig. 1*.

Table 2. The table of different pavement parameter settings

Ground	Asphalt	Heat flux: 53.3(W/m^2)
	Grass	Heat flux: 274.66(W/m^2); Energy dissipated: 64.2831(W/m^2)
Building		Volume:10m×10m×20m; Material : RC Wall; Wall thickness: 0.155m; Thermal conductivity: 3.78(W/m^{2}K); Heat flux: 0.61(W/m^{2}K)
Vegetation	Street Greening	Pore size:0.6; Permeability: 0.00009; Thermal conductivity coefficient: 0.13; Energy required for dissipation: (T1：3017.402W), (T5：5554.085W)
	Backyard Greening	Pore size:0.6; Permeability:0.00009; Thermal conductivity coefficient :0.13; Energy required for dissipation: (T1：1229.312W),(T5：2262.775W)

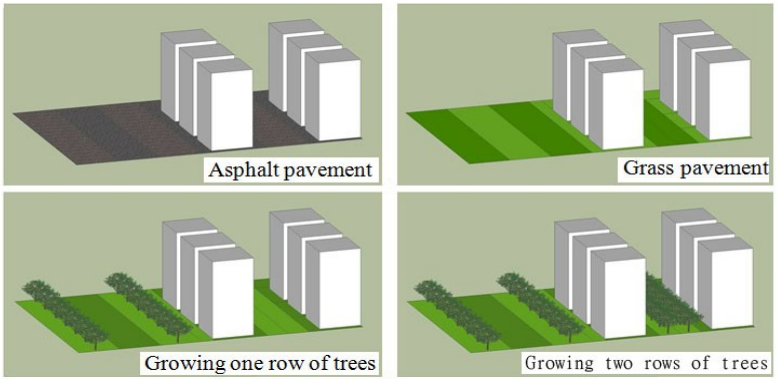

Figure 1. The simulation illustration of different pavement types

4. RESULTS AND DISCUSSIONS

This research simulated and analyzed how the temperature is influenced by vegetation dissipation, different wind speed and wind permeability. The results of each scenario are shown in the temperature line chart to compare the temperature influence by each factor.

Table 3. The table of the evapotranspiration of each pavement under different wind speed

Windless State	Asphalt (ori. state)		Windy State	Asphalt (ori. state)	
				Asphalt (windy)	
	Grass	With (w/o) evapotranspiration		Grass	With (w/o) evapotranspiration
	One row of trees	With (w/o) evapotranspiration		One row of trees	With (w/o) evapotranspiration
	Two rows	With (w/o)		Two	With (w/o)

	of trees	evapotranspiration	rows of trees	evapotranspiration

4.1 The influence of evapotranspiration on thermal environment temperature reduction

Generally speaking, the wider the vegetation area is, the larger the evapotranspiration becomes, which generate more cold air sources to reduce the temperature of the surroundings (Flor et al., 2004). In the research we compared the temperature reduction effectiveness by evapotranspiration in each wind field under the original state of windless and asphalt pavement condition and the temperature line chart for each state and the original state was plotted in a point-to-point way regarding the simulation of pedestrian wind field under two scenarios: 1.) the wind field penetrates the buildings *(Fig. 2)* and 2.) the wind field penetrates the streets *(Fig. 3)*. The analysis result is as follows:
In *Fig. 2* and *Fig. 3*, the observation point A is located on the sidewalk 1.5m ahead of the building group (X=31.5m), point B is located in the backyard of the building 1.5m ahead of the second row of building (X=57.5m) and point C is located 3m behind the building group (X=72m). In the comparison we found that there is a significant high temperature phenomenon behind the first row of building (point B) with vegetation pavement under a windless condition, where the highest temperature was observed in the condition of planting a row of trees (+8.37°C), while the grass pavement condition was inapparent in the temperature rising. In a windy environment, the average temperatures were all lower than the original state, where the lowest temperature zone was observed in front of the building group (X=20m) under the condition of planting two rows of trees, while the lowest temperature (-7°C) was found in the grass pavement condition behind the building group (X=72m).

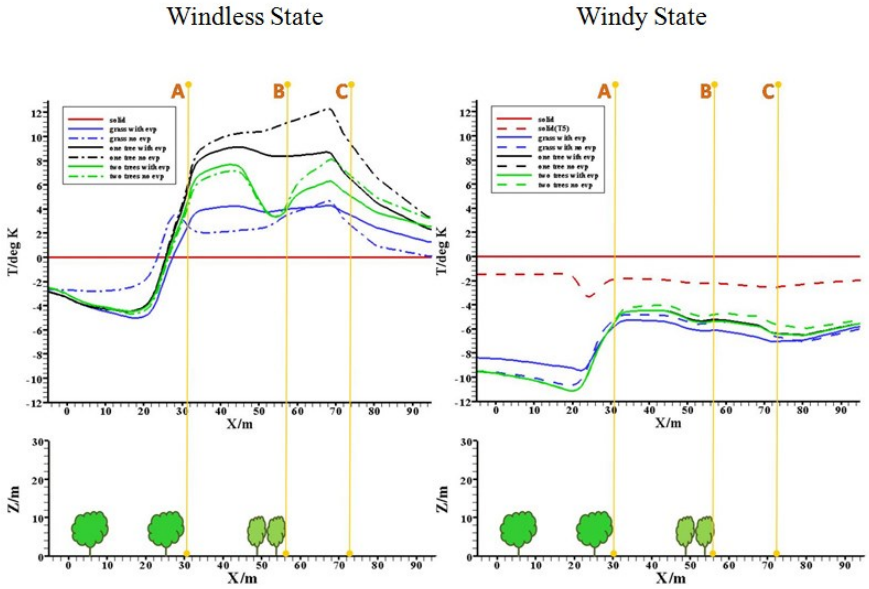

Figure 2. The comparison chart of the temperature difference for each pavement and the original state (asphalt) when the wind field penetrates the streets (y=16.5m)

Regarding the vegetation evapotranspiration (Picot et al., 2004), the temperature rising is more apparent without evapotranspiration in contrast to with evapotranspiration in each kind of pavement under a windless condition, where the temperature difference due to evapotranspiration in the condition of planting a row of trees reached 2.86°C (point B) and there is also a difference of

3.02°C behind the building group (point C). In a windy state the wind field helps reduce the temperature of the asphalt pavement and the situation is more apparent with evapotranspiration in contrast to a windless and non-evapotranspiration condition regarding the grass and vegetation pavement (Robitu et al., 2006). Thus, the evapotranspiration of vegetation pavement could bring the water into the flow field to reduce the surrounding temperature.

Table 4. The comparison table of the temperature difference for each pavement and the original state (asphalt) when the wind field penetrates the streets (y=16.5m)

	Windless State					Windy State			
		A	B	C			A	B	C
Asphalt	T1	0	0	0	Asphalt	T1	0	0	0
	T5	×	×	×		T5	-1.8	-2.19	-2.5
Grass	With evapotranspiration	2.53	4	3.64	Grass	With evapotranspiration	-5.65	-6.13	-7.05
	W/O evapotranspiration	2.61	3.6	2.95		W/O evapotranspiration	-5.04	-5.33	-6.59
One row of trees	With evapotranspiration	5.54	8.37	6.81	One row of trees	With evapotranspiration	-5.27	-5.2	-6.37
	W/O evapotranspiration	6.15	11.23	9.83		W/O evapotranspiration	-5.04	-4.7	-5.57
Two rows of trees	With evapotranspiration	4.61	4.16	5.3	Two rows of trees	With evapotranspiration	-5.26	-5.36	-6.39
	W/O evapotranspiration	4.29	4.72	7.07		W/O evapotranspiration	-5.05	-4.7	-5.58

Unit: (°C)

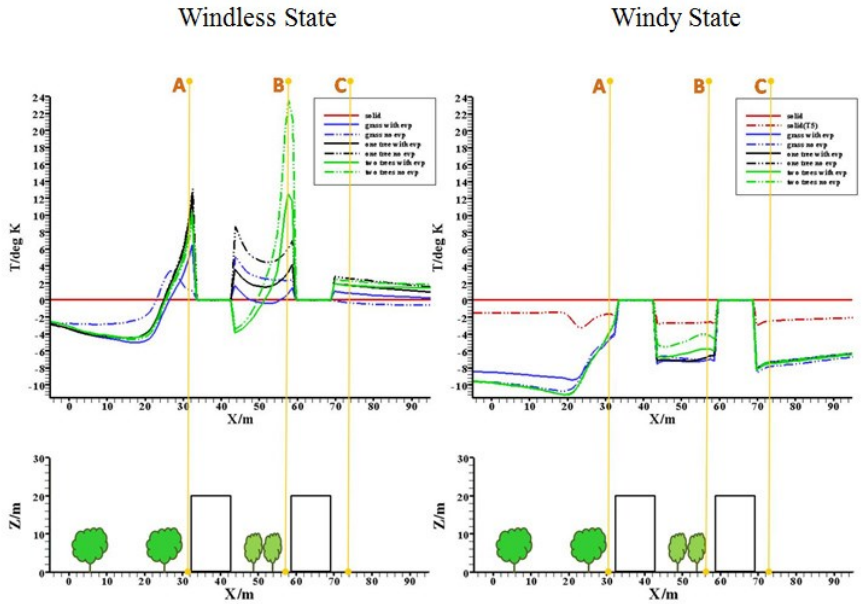

Figure 3. The comparison chart of the temperature difference for each pavement and the

original state (asphalt) when the wind field penetrates the buildings (y=23m)

Table 5. The comparison table of the temperature difference for each pavement and the original state (asphalt) when the wind field penetrates the buildings (y=23m)

	Windless State					Windy State			
		A	B	C			A	B	C
Asphalt	T1	0	0	0	Asphalt	T1	0	0	0
	T5	×	×	×		T5	-1.8	-2.19	-2.5
Grass	With evapotranspiration	4.82	0.73	0.81	Grass	With evapotranspiration	5.64	-6.12	-7.05
	W/O evapotranspiration	1.21	2.37	-0.22		W/O evapotranspiration	-5.04	-5.33	-6.58
One row of trees	With evapotranspiration	9	3.28	1.76	One row of trees	With evapotranspiration	-5.26	-5.23	-6.36
	W/O evapotranspiration	9.85	6.23	2.63		W/O evapotranspiration	-5.04	-4.7	-5.59
Two rows of trees	With evapotranspiration	7.72	12.48	1.75	Two rows of trees	With evapotranspiration	-5.26	-5.36	-6.39
	W/O evapotranspiration	7.24	23.57	2.32		W/O evapotranspiration	-5.05	-4.7	-5.58

Unit: ℃

4.2 The influence of wind speed on each kind of pavement

According to the simulation data, the wind field makes the air flow better in the urban environment and results in a larger temperature reduction. From Fig. 4 we see an apparent temperature reduction effect n the windy state in each kind of pavement, among which the planting two rows of trees has 7.04°C drop, followed by the planting one row of trees with 7.01°C drop. Thus it can be seen that the wind field blowing could bring a good and apparent temperature reduction effect for the urban environment.

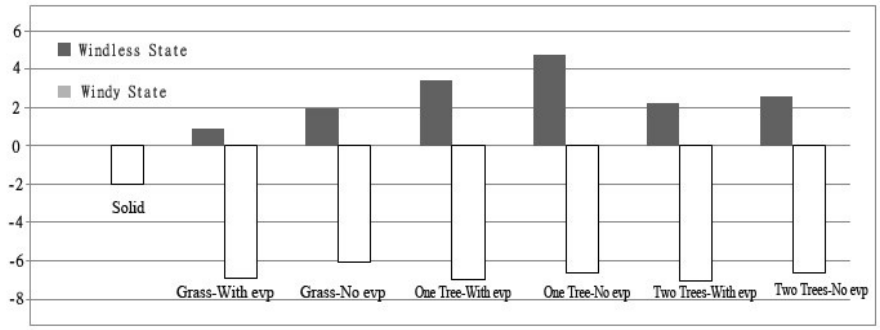

Figure 4. The comparison chart of the temperature difference between each pavement and the original state (asphalt) in the pedestrian wind field

4.3 The influence of urban environment permeability on the temperature field

From *Table 4* and *5* we can see that the flow stream distribution of the wind field and the temperature change are interfered by the buildings. In the more penetrable streets, despite the wind field is affected by the surrounding buildings,

the high temperature situation is less severe with its penetrability. *Table 6* is the comparison table shows the generated highest temperature of each pavement under the condition of being blocked by the buildings and in the street wind field. The result indicates that the highest temperature in the street is lower than that of being blocked by the buildings, which suggests that a well-ventilated environment facilitates the temperature reduction effect (Huang et al., 2005); also we found that planting two rows of trees appears the best temperature reduction effect, which implies that the vegetation arrangement shall be accompanied with a well-ventilated environment to soothe the urban high temperature phenomenon with wind field blowing.

Table 6. The comparison table of the generated highest temperature of each pavement in the buildings and streets

	Pavement type	Asphalt	Grass	One row of trees	Two rows of trees
Windless State	y=23	40.58	41.96	47.07	51.41
	y=16.5	39.15	42.83	47.09	44.79
	Temp. Diff.	-1.43	0.87	0.02	-6.62
Windy State	y=23	37.7	33.58	32.57	33.4
	y=16.5	36.89	33.56	32.73	32.7
	Temp. Diff.	-0.41	-0.02	0.16	-0.7

Unit: (°C)

5. CONCLUSION

This research explored the temperature reduction effect generated by the evapotranspiration of pavement and vegetation arrangement under different wind state and introduced CFD numerical simulation method to analyze the influence of different wind field (windless and windy), pavement arrangement (asphalt, grass, street greening, street greening and backyard greening behind building) and evapotranspiration (with or w/o) etc. on wind speed, temperature and heat energy. The result is concluded as the following items.

The water generated by the vegetation evapotranspiration in the urban environment could decrease the temperature of the surroundings and soothe the high temperature phenomenon, while the temperature reduction is in apparent without evapotranspiration.

With the blowing of wind field, the cold air is formed by the evapotranspiration of each pavement and influences the surrounding high temperature area to improve the environmental thermal comfort by reducing 4°C-6°C in average under a windy condition.

Comparing the temperature reduction effect with the original state, the grass and vegetation pavement could facilitate the temperature reduction effect. And since the grass pavement has better wind field penetration than the vegetation pavement which blocks the wind field flowing, there is a significant temperature reduction effect between the buildings.

The vegetation evapotranspiration provides water content to the environment to reduce the surrounding temperature and the effect would become more apparent if it is accompanied with smooth wind field. Therefore, the vegetation arrangement shall be considered together with well-ventilated environment in order to soothe the urban high temperature phenomenon with the wind field blowing.

In the urban environment, the heat tends to accumulate on the lee side of the building due to slow wind speed. The flow field is nearly static in the windless state, which makes it difficult for heat dissipation and results in high temperature

and poor temperature reduction effect.

In the urban design, the vegetation arrangement shall not only considers the visual beautification of the landscape, but also the functions of wind flow and temperature reduction to improve the environmental comfort in a nature way. Regarding the urban design code for vegetation and pavement arrangement, this research refer to the temperature reduction effect on hot environment induced by the evapotranspiration of vegetation and pavement in the urban area and propose the following suggestions:

The evapotranspiration of vegetation has temperature reduction effect on urban hot environment and the effect could become more apparent with the blowing of the wind field. Hence, for the future vegetation design we shall consider the building arrangement and the different wind direction to create a good wind blowing effect in the urban space and achieve the purpose of reducing the surrounding high temperature.

Since the grass pavement has higher penetrability and less interference to the smooth blowing of the wind field, a good temperature reduction effect could be obtained. We suggest introducing more nature pavement materials in future urban design to increase the water content of the ground, which could provide cold air sources for the urban high temperature environment and improve the environmental thermal comfort.

Since the windward and lee side of the building and the pedestrian wind filed are all observed the significant heat accumulation condition, we suggest to consider the ventilation effect in the building's arcade design to remove the accumulated heat on the building surface as well as the pedestrian wind field via the wind field.

AKNOWEGMENT

This study was funded by the National Science Council (NSC 101-2627-E-027-002-MY3). We are deeply grateful for the support provided.

REFERENCES

Allen, R.G., Pereira, L.S., Raes, D., Smith, M. (1998). "Crop evapotranspiration, guidelines for computing crop water requirements", *FAO Irrig. and Drain. Paper 56,* 300, Food and Agric. Orgn. of the United Nations, Rome, Italy.

Arnfield, J. (2003). "Review two decades of urban climate research: A review of turbulence, exchanges of energy and water, and the urban heat island", *Int. J. Climatol*., 23, 1-26.

Baskaran, A. and Kashef, A. (1996). "Investigation of air flow around buildings using computational fluid dynamics techniques", *Engineering Structures,* 18(11), 861-875.

Bittelli, M., Ventura, F., et al. (2008). "Coupling of heat, water vapor, and liquid water fluxes to compute evapotranspiration in bare soils", *Journal of Hydrology,* 191-205.

Fahmy, M., Sharples, S., et al. (2010). "LAI based trees selection for mid latitude urban development: A microclimatic study in Cairo, Egypt", *Building and Environment,* 45(2), 345-357.

Flor, F.S. de la and Dom´ınguez, S.A. (2004). "Modelling microclimate in urban environments and assessing its influence on the performance of surrounding buildings", *Energy and Buildings,* 36(5), 403-413.

Giridharana, R., Laua S.S.Y., et al. (2007). "Urban design factors influencing heat island intensity in high-rise high-density environments of Hong Kong", *Building and Environment*, 42(10), 3669-3684.

Golany, G.S. (1996). "Urban design morphology and thermal performance", *Atmospheric Environment,* 30(3), 45-65.

Gromke, C. and Ruck, B. (2007). "Influence of trees on the dispersion of pollutants in an urban street canyon—Experimental investigation of the flow and concentration field", *Atmospheric Environment,* 41, 3287-3302.

Hang, J., Li, Y., et al. (2010). "Wind conditions and ventilation in high-rise long street models", *Building and Environment,* 45, 1353-1365.

Huang, H., Ooka, R., et al. (2005). "Urban thermal environment measurements and numerical simulation for an actual complex--urban area covering a large district heating and cooling system in summer", *Atmospheric Environment,* 39, 6362-6375.

Lin, B., Li X.F., et al. (2008). "Numerical simulation studies of the different vegetationpatterns' effects on outdoor pedestrian thermal comfort", *Journal of Wind Engineering and Industrial Aerodynamics*, 96(10-11), 1707–1718.

Lin, T.P., Dear, R. de, et al. (2011). "Effect of thermal adaptation on seasonal outdoor thermal comfort", *Int. J. Climatol.,* 31, 302–312.

Picot, X. (2004). "Thermal comfort in urban spaces: impact of vegetation growth Case study: Piazza della Scienza, Milan, Italy", *Energy and Buildings,* 36(4), 329-334.

Robitu, M., Musy, M., et al. (2006). "Modeling the influence of vegetation and water pond on urban microclimate", *Solar Energy,* 80(4), 435-447.

Tang, C., Hsu, S.H., et al. (2007). "Comparison of Different Methods in Evapotranspiration Estimation from St. Augustine Pasture", *Crop, Environment & Bioinformatics,* 4, 151-160.

Wang, Y., Liu, H., et al. (2005). "Study on Carbon Dioxide Fixation Efficiency of sidewalk trees Alstonia scholaris", *Quarterly Journal of Chinese Forestry,* 38(3), 279-290.

International review for spatial planning and sustainable development, Vol.1 No.4 (2013), 13-28
ISSN: 2187-3666 (online)
DOI: http://dx.doi.org/10.14246/irspsd.1.4_13
Copyright@SPSD Press from 2010, SPSD Press, Kanazawa

The Carbon Footprint Calculation of the GFRP Pedestrian Bridge at Tai-Jiang National Park

Yeou-Fong Li[1*], Chung-Cheng Yu[1], Syun-Yu Chen[1], Badjie Sainey[1]
1 Department of Civil Engineering, National Taipei University of Technology
** Corresponding Author, Email: yfli@ntut.edu.tw*
Received 7 Feberuary 2013; Accepted 7 August 2013

Keywords: Glass Fiber Reinforced Plastics, Pedestrian Bridge, Carbon Footprint

Abstract: This paper proposes a study of a high strength, light weight and durable glass fiber reinforced polymer (GFRP) composite material that was used in a pedestrian bridge in Tai-Jiang National Park, Taiwan. In order to better understand the carbon footprint and carbon reduction of GFRP pedestrian bridge, the evaluated carbon footprint of the superstructure of the GFRP pedestrian bridge is compared with those of traditional construction materials, such as reinforced concrete (RC) and steel. The evaluation includes material production stage, transportation stage and construction stage of the carbon emission of GFRP pedestrian bridge. From the calculated carbon emission results, it is found that the GFRP pedestrian bridge reduced total carbon emission about 43% compared to an RC pedestrian bridge and up to 19% compared to a steel pedestrian bridge.

1. INTRODUCTION

FRP composite materials have excellent durability and fatigue resistance properties. When used as a structural material, FRP members exhibit high strength, light weight, great corrosion resistance and other excellent mechanical properties. In this paper, glass fiber reinforced polymer (GFRP) composite material was used to build a pedestrian bridge in Tai-Jiang National Park, Taiwan, located in a high salinity coastal area where the conventional reinforced concrete or steel structures were vulnerable. The reason for using GFRP composite material in Tai-Jiang National Park is due to the high chloride erosion environment resulting in severe corrosion of the reinforced concrete and steel. Therefore, a GFRP pedestrian bridge was proposed, which will reduce the subsequent maintenance cost compared to the reinforced concrete and steel bridges because of the excellent durability performance.

The construction of a pedestrian bridge in the National Park must take into account the impact on the environment and landscape of the park. The rising environmental awareness in recent years calls for energy saving and carbon dioxide emission reduction to complement the national goals. Environmental consideration in various construction projects has become increasingly important, especially in traditional civil engineering and construction methods with high carbon dioxide emissions, so reducing such emissions are becoming a trend all over the world. Therefore, this paper introduces the GFRP pedestrian bridge's mechanical experiment, structural design, deflection analysis, strength analysis and mechanical properties to suggest an alternative to traditional structures. The carbon footprint (total

carbon dioxide emission) of the GFRP pedestrian bridge was also calculated for the production stage, the transportation stage. The carbon footprint of the reinforced concrete and steel pedestrian bridges are also investigated and compared with the GFRP pedestrian bridge.

2. LITERATURE REVIEW

The following references were consulted for the analysis of the GFRP components, and some practical application cases in the GFRP pedestrian bridge

2.1 Literature Review of GFRP Components

Davalos et al. (1996) proposed the flexural deformation and strain of different type I and box section GFRP components, by using the three-point and four-point bending tests, a hierarchical system theory, mechanics of laminated beams, and finite element analysis. Qiao et al. (2000) made a single-span GFRP composite bridge. The analysis and design of the GFRP composite bridge, and the experimental and finite-element numerical model were proposed. A series of approximate solutions were used in the analysis and design of GFRP bridge system also. Neto and Rovere (2007) considered the design and analysis of GFRP pultruded wide flanged I-beam under bending by using three-point bending test, numerical analysis, and Timoshenko beam theory. Four GFRP beams of different spans were used to determine the elastic modulus and shear modulus, and the force-displacement diagrams give a similar stiffness value for the numerical, analytical and experimental results.

Li and Kan (2011) present the mechanical behaviors of hybrid fiber reinforced plastic (HFRP) composite beams. Three-point bending test was conducted to obtain the force-displacement relationship, stiffness and failure strength of the GFRP beams. The test results show that the stiffness of GFRP beam filled with epoxy mortar is twice as large as GFRP beam without epoxy mortar. The Timoshenko beam theory and the finite-element analysis were used to calculate the force-displacement relationship of the GFRP beams. After comparison, the experimental results and the numerical and analytical results are quite close to each other. Li et al. (2012) present the use of GFRP composite bridge deck subjected to three-point bending test to determine the mechanical behaviors as well as the failure modes. Test results were compared with the results taken from finite-element method analysis software to verify the accuracy of the finite-element model. The finite element analysis results had a relative error of 12.8 % compared to the experimental result.

2.2 Examples of GFRP Bridges

Some FRP pedestrian bridge will be introduced as follows. Near Kentucky University in the U.S., there is an GFRP pedestrian bridge 18.29 *m* long and 1.83 *m* wide. The two girders of the structure are composed of glass fiber, carbon fiber and Vinyl resin. Prestressed cables were fixed into the flanges of the I-beam and the CFRP bridge deck with the purpose of increasing the beam bending stiffness in order to meet the design load requirement of 415 kgf/m^2 and allowable deflection of $L/180$.

Neal Bridge located in Maine, U.S., is an arch bridge with a span of 8.1 *m*, a length of 10.2 *m* and a width of 13.5 *m*. Thin-walled CFRP composite tubes of diameters ranging from 23~30.5 *cm* were filled with concrete to construct the arch bridge. The concrete took the compression force while the thin-walled CFRP tubes provide confinement to the concrete.

Okinawa Road Park Bridge is an GFRP pedestrian bridge located in Okinawa Prefecture, Japan. The construction of the bridge was completed in 2001 and it is about 38 *m* in length, and 4.5 *m* in width. Okinawa Prefecture is surrounded by the sea and harsh corrosion environment; therefore, the area takes much interest in corrosion resistance GFRP composite components for construction. The bridge is made of a two-span continuous girder structure resting on an RC wall pier. The main girders are GFRP panels made by hand lay-up and cross frame, and the GFRP bridge decks are made by pultrusion (Nayomon and Kitayama, 2003).

A two-span GFRP pedestrian bridge was constructed in 2011 in the recreational area of the Yangmingshan National Park, Taipei, Taiwan. The bridge measures a total length of about 8 *m* and width of 1.2 *m*. GFRP components were used to build the bridge in the harsh environmental conditions of the National Park because of its lightweight, easy of construction and high corrosion resistance properties. After laboratory experiments confirmed the many advantages of GFRP, the construction and assembly of the bridge with simple hand tools were completed within three days. This dramatically reduced the impact on the environment; moreover, the use of GFRP overcame the corrosion problem of traditional materials, thus reducing post-maintenance costs.

3. STRUCTURAL DESIGN OF GFRP PEDESTRIAN BRIDGE

The design concept of the GFRP pedestrian bridges refers to the codes of some countries, such as Japan (Composite structure of Society of Civil Engineers Committee, 2011), and U.S. (U.S. Department of Agriculture, Forest Service, Technology and Development Program, 2011; American Association of State Highway and Transportation Officials ASSHTO, 2008), and then follows the Design Specifications for Highway Bridge issued by the Ministry of Transportation and Communications, Taiwan. The three-point bending test results of GFRP members were considered in designing the structure of the bridge. Consequently, the physical and chemical properties of GFRP materials were compared with those provided by the manufacturer of the GFRP components to be employed as the basis of the structural design and safety check of the GFRP pedestrian bridge.

3.1 Test Methods

The three-point bending test of the main girder of the GFRP pedestrian bridge is done using a 500-*ton* universal testing machine, shown in *Figure 1*. The mechanical testing of the 6 *m* span specimen labeled H410-L6 is based on displacement control. The component was loaded at midpoint at a downward displacement rate of 1 cm/min. The loading of specimen H410-L6 was stopped when the mid-point displacement reached a value of 2 *cm*.

Figure 1. A 6 *m* span length of H410-L6

From the test results obtained from the force-displacement relationship diagram, the midpoint flexural deformation of 2 *cm* with a corresponding force of 26.7 *kN* (shown in *Figure 2*) is used to calculate the stiffness of the specimen, as shown in *Table 1*.

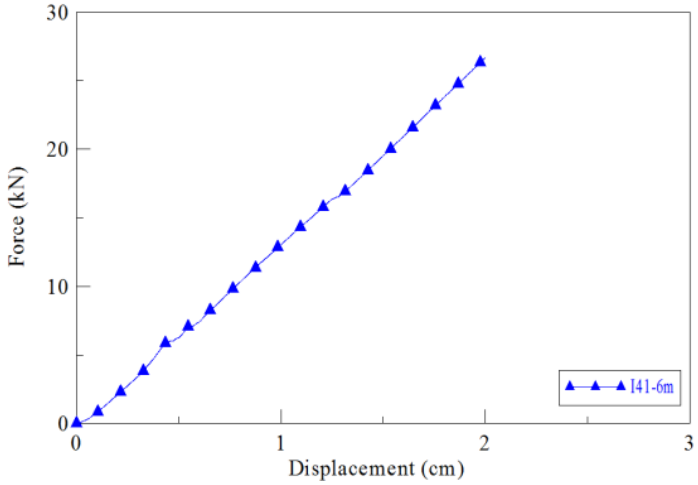

Figure 2. The force-displacement relationship of specimen H410-L6

Table 1. Three-point bending *test* result of specimen H410-L6

Specimen	Midpoint deformation (*cm*)	Corresponding force (*kN*)	Stiffness (*kN/cm*)
H410-L6	2	26.7	13.35

Test results are then compared with the analytical value, using Euler beam theory to obtain the force–displacement relationship. In the three-point bending test, a concentrated load was applied at mid-span of the component, and the corresponding Euler beam equation is given for H410-L6 as Eq. (1) below:

$$\delta = \frac{PL^3}{48EI} \tag{1}$$

where P is the applied force and I is the section modulus of inertia. From Eq. (1), the resulting elastic modulus of the specimen H410-L6 can be calculated, $E = PL^3 / 48\delta I = 180,823.5\, kgf / cm^2$ 。

The experimental result of the elastic modulus is only 3.3% more than the value of elastic modulus, 175,000 *kgf/cm*^{2}, provided by the manufacturer. In general, the three-point bending test result and the theoretical calculations indicate that the material properties provided by the GFRP manufacturer of H410-L6 have a relatively high accuracy.

3.2 Structural Design

The superstructure of the GFRP pedestrian bridge uses Glass Fiber Reinforced Plastic (GFRP) composite material components connected to each other either chemically by adhesive resins, or by a mixture of adhesive resins and GFRP bolts. The following describes the structural design of each item employed in the superstructure:

The main GFRP beam is designed using four single web I-beams, 20 *cm* wide, 41 *cm* high, and 800 *cm* in total length. As shown in *Figure 3*, GFRP diaphragms are placed in-between the four I-beams at 1/4, 1/2 and 3/4 of the length of the I-beam with the intention of resisting the shear force and transmitting the applied force to the other adjacent I-beams. A total of 16 GFRP composite decks, each 150 *cm* long, 50 *cm* wide and 1.2 *cm* thick, are used. These are connected to the girders of the diaphragm by GFRP bolts and adhesive respectively.

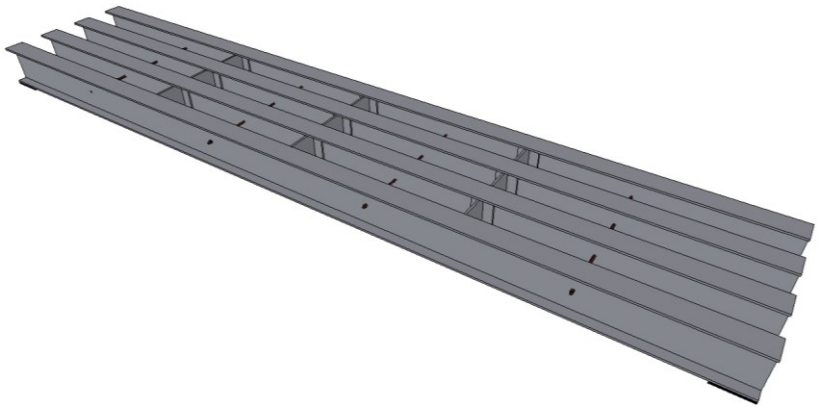

Figure 3. The illustration diagram of I beams and diaphragms of the GFRP pedestrian bridge

3.3 Deflection Check of the GFRP Pedestrian Bridge

This FPR pedestrian bridge deck was designed assuming a pedestrian live load of 400 *kgf/m*^{2}. In the other calculations, the stress impact from the sidewalk live load was neglected. With regards to the deflection control requirements, reference was made on the GFRP design specifications and recommendations from the United Kingdom, the United States, as well as

Japan and other countries. In this paper, we adopted the United States regulation for the deflection, i.e., the limit deflection value of *L*/300.

Using the Euler beam formula of Eq. (2) below, we found that the 750 *cm* span GFRP girder of the pedestrian bridge had a maximum displacement value of 1.65 *cm* for a live load of 2.12 *kgf/cm* and the dead load is 0.108 *kgf/cm*.

$$\delta = \frac{5wl^4}{384EI} \tag{2}$$

The maximum allowable deflection from the design code, *L*/400 (1.87 *cm*), is 14.3 % larger than the design GFRP pedestrian bridge. Nakamura et al. (2012) proposed the maximum allowable deflection (*L*/500) is found to be approximately 1.5 *cm*.

3.4 Safety Check of the GFRP Pedestrian Bridge

It is relevant to make sure that the GFRP bridge fulfills the deflection control design standards in order to provide sufficient comfort to users and, more importantly, to ensure that the GFRP pedestrian bridge provides its users with adequate safety. In order to check the strength of the bridge, the ultimate strength of the material provided by the manufacturer, the girder component's geometry and cross section corresponding to the shear and moment diagrams of the GFRP girder (see *Figure 4*) due to the load applied were used to check the strength.

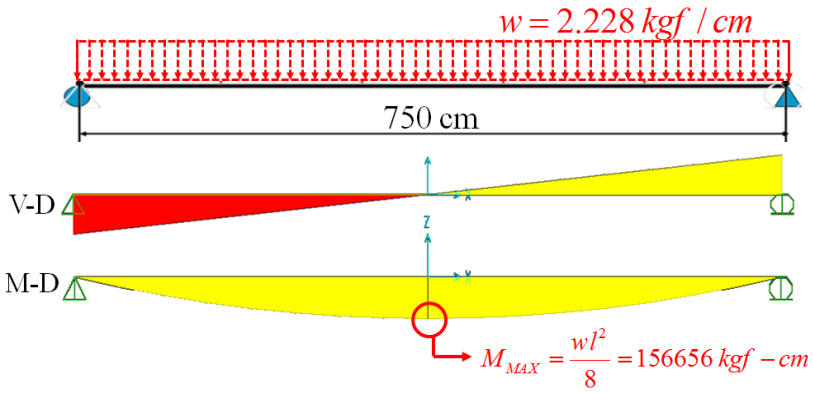

Figure 4. The shear and moment diagrams of the GFRP girder

The maximum bending moment required of the GFRP girder under full loading is found from Eq. (3) as 156,656 *kgf-cm* while the allowable moment value is shown in Eq. (4). Therefore, the safety factor (SF) of the GFRP pedestrian bridge in this study, calculated from Eq. (5), is found to be up to 20.4. This safety factor shows that designing the GFRP pedestrian bridge using the deflection control of *L*/300 provides users with sufficient safety.

$$M_{MAX} = \frac{wl^2}{8} \tag{3}$$

$$M_{all} = \frac{\sigma I}{y} \tag{4}$$

$$S.F. = \frac{M_{all}}{M_{\max}} \tag{5}$$

4. Carbon footprint Calculation

Based on the "Guidelines for carbon footprint calculation of products and se ıe
ca re
at

4

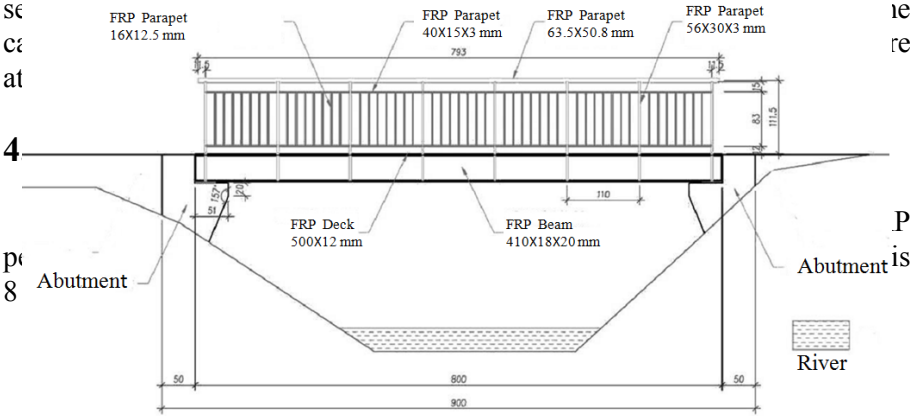

P
pe is
8

Figure 5. The illustration diagram of GFRP pedestrian bridge at Tia-Jiang National Park

4.2 Evaluation Flowchart

In this study, the production stage, transportation stage and construction stage of the superstructure of the GFRP pedestrian bridge were considered. The evaluation flowchart is shown in *Figure 6*.

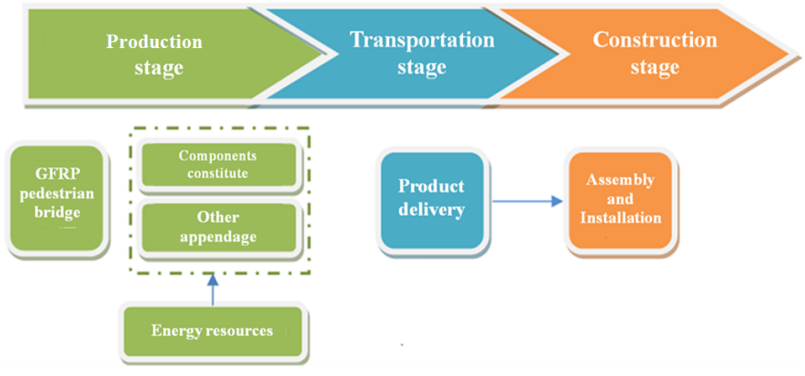

Figure 6. The evaluation flowchart of Tia-Jiang Park GFRP pedestrian bridge

4.3 Inventory Data and Calculation

In this paper, the carbon footprint inventory items of the GFRP pedestrian bridge includes the production stage, delivery of the materials to

the site, assembly stage of the components as well as the energy consumed in the whole process, as shown in *Table 2*. The carbon footprint inventory data of GFRP pedestrian bridge of carbon dioxide emissions was taken from the SimaPro database, complemented by carbon emission coefficient obtained from domestic and foreign databases (Hsu *et al.*, 2011; Hu *et al.*, 2011).

Table 2. The calculation of the carbon dioxide emission of the GFRP pedestrian bridge

Evaluation stage	Item		Input value	Unit	Carbon emission coefficient	Calculated result ($kgCO_2eq$)
Production	GFRP component	Glass fiber	785.97	*kg*	2.63 $kgCO_2eq/kg$*	2,067.11
		Epoxy resin	428.71	*kg*	6.72 $kgCO_2eq/kg$*	2,880.95
	Rubber pad		16.65	*kg*	3.18 $kgCO_2eq/kg$**	52.96
	Structural adhesive		2.20	*kg*	15.20 $kgCO_2eq/kg$*	33.44
	Resin		5.60	*kg*	6.72 $kgCO_2eq/kg$*	37.63
	Paint		73.64	*kg*	3.56 $kgCO_2eq/kg$**	262.17
Summation						5,334.24
Transpor-tation	Products delivery (Total weight of GFRP components 1.214 *t*; distance from Taichung to Tainan approx. 160 *km*)		194.35 (=1.214 ×160)	*t·km*	0.33 $kgCO_2eq/t \cdot km$*	64.33
Summation						64.33
Construc-tion	Electricity (power consumption of crane hoisting the diaphragm into position)		82.35	(*kwh*)	0.81 $kgCO_2eq/ kwh$*	66.70
	(Total weight of 25 *t*; a return trip distance of 50 *km*)		1,250 (=25 × 50)	*t·km*	0.33 $kgCO_2eq/t \cdot km$*	413.75
Summation						480.45
Total						5,879.02

* Unit amount of CO_2 emissions data taken from SimaPro software
** Unit amount of CO_2 emissions data taken from INVENTORY OF CARBON & ENERGY (ICE), Version 1.6a (Hammond and Jones, 2008).

The three different stages of the superstructure of the GFRP pedestrian bridge produced a total of 5,879 $kgCO_2eq$. The production stage accounted for 91% carbon dioxide emission, making it the largest in the assessment, while the transportation stage and construction stage accounted for only 1% and 8% respectively. The carbon emission of the GFRP pedestrian bridge for the different stages is shown in *Figure 7*.

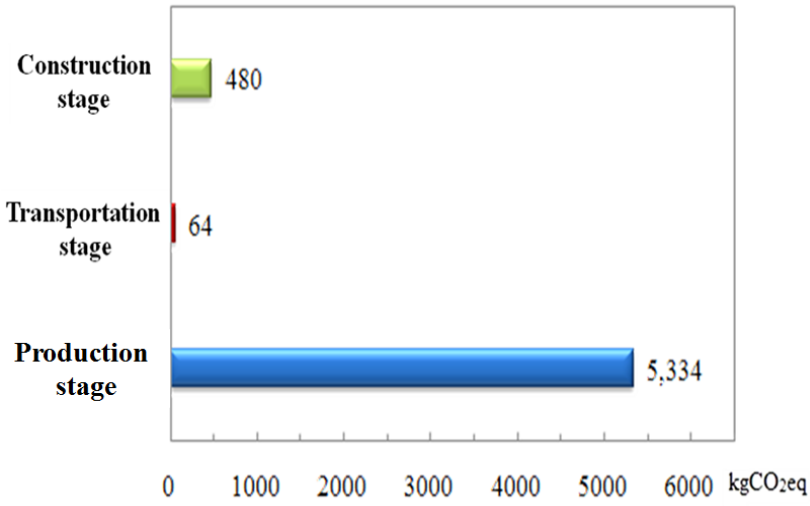

Figure 7. The carbon dioxide emission of the GFRP bridge for different stages

5. Benefit analysis

In order to explore the carbon footprint and carbon dioxide reduction benefits of the GFRP pedestrian bridge; the reinforced concrete and steel bridges were adopted and compared. The structural design of the two types of bridge structures were taken into account to meet the design code and providing the same service performance of the GFRP pedestrian bridge.

5.1 Reinforced Concrete Pedestrian Bridge

For the RC pedestrian bridge, the actual existing conditions of a high salinity in the Tai-Jiang Park environment is considered for the design and according to design specifications, a concrete cover of at least 6.5 *cm* in thickness is required to protect the reinforcement inside the concrete. Minimum concrete compressive strength of 350 kgf/cm^2 and minimum steel yield strength of 4,200 kgf/cm^2 were used. *Figure 8* is a sectional diagram of the RC pedestrian bridge.

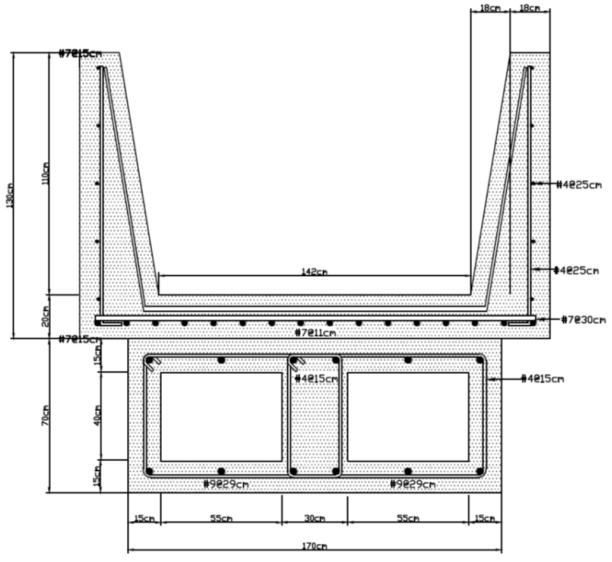

Figure 8. The cross section of the RC pedestrian bridge

Similar to that of the GFRP pedestrian bridge, the production, transportation and construction stages are calculated. The carbon dioxide emission of the RC pedestrian bridge for different stages is shown in *Table 3* as follow.

Table 3. The calculation of the carbon dioxide emission of the RC pedestrian bridge

Evaluation Stage	Input Item	Input value	Unit	Carbon emission coefficient	Calculated result ($kgCO_2eq$)
Production	Concrete	12,817.54	*kg*	0.21 $kgCO_2eq/kg$**	6,782.74
	Reinforcement	779.95	*kg*	1.45 $kgCO_2eq/kg$*	1800.54
Summation					8,583.28
Transportation	Concrete delivery (Concrete total weight of 1.138 *t* from Taiwan Concrete Factory, Ren-Wu Branch, local distance of 70.2 *km*)	2,267.46 (=32.298 ×70.2)	*t*·*km*	0.33 $kgCO_2eq/\ t \cdot km$*	750.53
	Transportation of reinforcement (Total weight of 1.241 *t* from Tong-Ho Steel, Kao-Hsiung to site, a distance of 88.4 *km*)	109.62 (=1.241× 88.4)	*t*·*km*	0.33 $kgCO_2eq/\ t \cdot km$*	36.28
Summation					786.81
Construction	Electricity	564	*kwh*	0.81 $kgCO_2eq/kwh$*	456.84
	Crane usage (Crane weighs 25 *t* and travels 50 *km* return trip from Tainan City)	1,250 (=25×50)	*t*·*km*	524.16$kgCO_2eq/\ t \cdot kmn$*	413.75
Summation					870.59
Total					10,240.68

* Unit amount of CO_2 emissions data taken from SimaPro software
** Unit amount of CO_2 emissions data taken from INVENTORY OF CARBON & ENERGY (ICE), Version 1.6a (Hammond and Jones, 2008).

The evaluation of the RC pedestrian bridge includes the production, transportation and construction stages. And the amount of carbon dioxide emissions of the three stages is 10,240.68 $kgCO_2eq$. The highest proportion of the carbon dioxide emissions is at the production stage, accounting for 84%, the transport stage accounted for 8%, while the construction stage accounted for 9%. The carbon emission of the steel pedestrian bridge for different stages is shown in *Figure 9*.

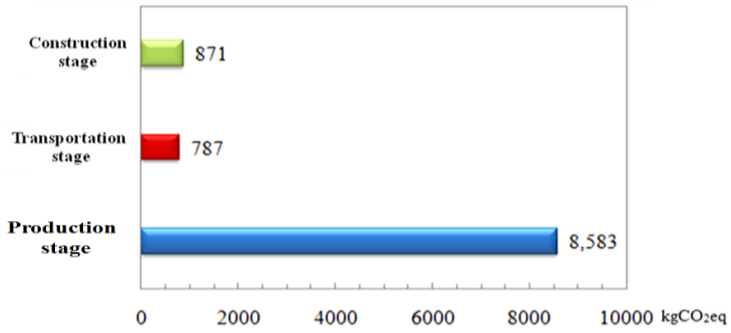

Figure 9. The carbon dioxide emission of the RC bridge for different stages

5.2 Steel Pedestrian Bridge

The designing of the handrail and deck of the steel pedestrian bridge deck handrail design is taken to be of the same or approximate cross-section as that of the GFRP pedestrian bridge. On the other hand, the main girders of the steel bridge use three single web I-beams that are 20 *cm* wide, 30 *cm* high and 800 *cm* in total length. A sectional view of the steel bridge is shown in *Figure 10*.

Also, in evaluating the carbon dioxide emission of the steel bridge, the production, transportation and construction stages are assessed in a similar way as the GFRP pedestrian bridge. The carbon dioxide emission of the RC pedestrian bridge for different stages is shown in *Table 4*.

The steel pedestrian bridge produced a total of 7,265 $kgCO_2eq$ for the three stages. The production stage accounted for 83% carbon dioxide emission making it the largest, while the transportation stage and construction stage accounted for only 1% and 16% respectively. The carbon dioxide emission of the steel pedestrian bridge for different stages is shown in *Figure 11*.

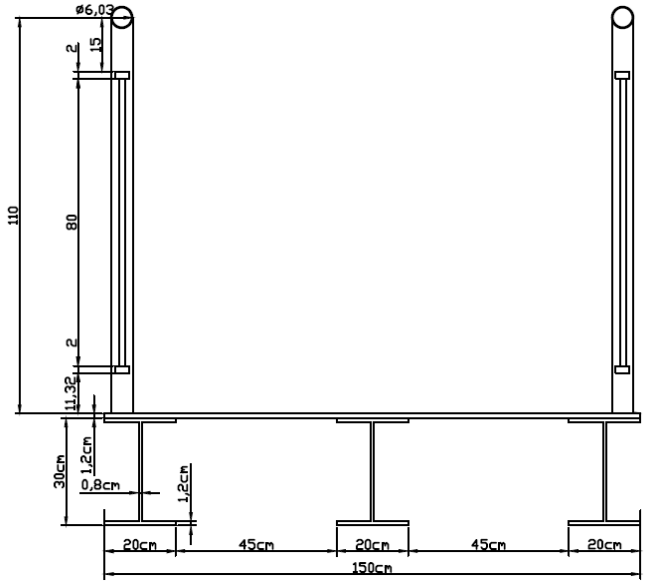

Figure 10. The cross section view of the steel pedestrian bridge

Table 4. The calculation of the carbon dioxide emission of the GFRP pedestrian bridge

Evaluation stage	Input items	Input value	Unit	Carbon emission coefficient	Calculated result ($kgCO_2eq$)
Production	Steel section	3,074.88	*kg*	1.77 $kgCO_2eq/kg$**	5,442.54
	Paint	73.64	*kg*	3.56 $kgCO_2eq/kg$**	262.16
	Bolts	200.00	*kg*	1.56 $kgCO_2eq/k$*	312.00
	Welding electrodes	264	*kg*	0.12 $kgCO_2eq/kg$*	31.68
Summation					6,048.38
Transportation	Steel beam transportation (Total weight of 3.074 *t* to be transported for 88.4 *km*, from Tung-Ho Steel, Kao-Hsiung to Tainan)	271.39 (=3.074× 88.4)	*t ·km*	0.33 $kgCO_2eq/t \cdot km$ *	89.93
Summation					89.93
Construction	Electricity	880	*kwh*	0.81 $kgCO_2eq/ kwh$	712.80
	Crane usage (Crane weight is 25 *t*, return trip from Tainan City is 50 *km*)	1,250 (=25×50)	*t·km*	0.33 $kgCO_2eq/ t \cdot km$*	413.75
Summation					1,126.55
Total					7,264.76

* Unit amount of CO_2 emissions data taken from SimaPro software
** Unit amount of CO_2 emissions data taken from INVENTORY OF CARBON & ENERGY (ICE), Version 1.6a (Hammond and Jones, 2008).

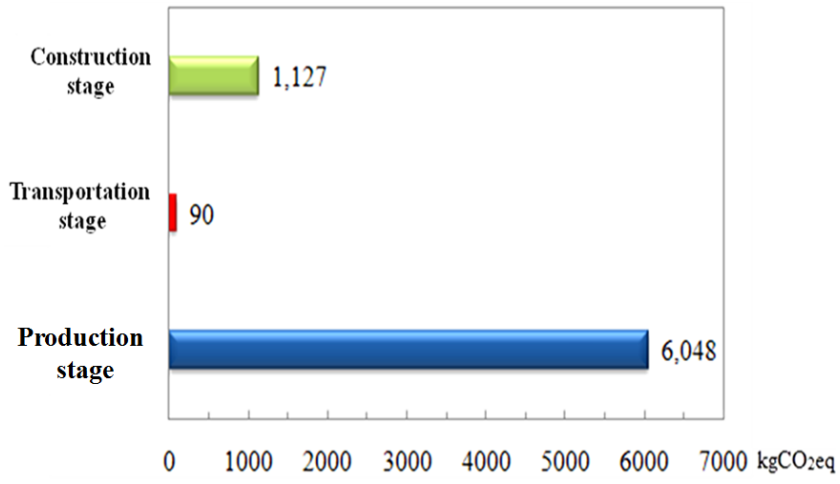

Figure 11. The carbon dioxide emission of the steel bridge for different stages

5.3 Benefit Analysis

The carbon reduction benefits of the superstructure of the GFRP pedestrian bridge and that of the traditional construction materials is calculated as follows.

Carbon dioxide equivalence reduction benefits=

[(*construction material* −*GFRP*) / *construction material*] (6)

The carbon emission in the production stage between the GFRP and the other two traditional construction materials had the largest difference. The reason is clearly because GFRP has the advantages of high strength and light weight. Thus, for the same design conditions, GFRP will use a smaller amount of material to provide the same service performance of a pedestrian bridge compared to the traditional construction materials. Comparatively, the RC pedestrian bridge will have carbon dioxide emissions of 3,249 $kgCO_2eq$ more than the GFRP pedestrian bridge, accounting for 38% carbon reduction for the GFRP. The steel pedestrian bridge, in a similar way, will produce carbon dioxide emissions of 714 $kgCO_2eq$ more than the GFRP pedestrian bridge and accounting for 12% carbon reduction.

In the transportation stage, although the finished GFRP components took a longer distance to be delivered, the GFRP pedestrian bridge is of lower density and thus weighs lighter when compared to a steel pedestrian bridge of the same handrail design cross section. Therefore in this stage, the RC bridge will produce 722 $kgCO_2eq$ more than a GFRP pedestrian bridge, accounting for 92% carbon reduction, while the steel bridge produces 26 $kgCO_2eq$ more carbon dioxide emission than the GFRP one accounting for 28% carbon reduction in the transportation stage.

When it comes to the construction stage, not much energy was needed or heavy machinery was required because the GFRP members were adhesively bonded to one another so a crane only can hoisting the GFRP pedestrian bridge into position. The other two traditional construction materials require a lot of heavy machinery and equipment for their construction. Steel needs electric welding to join its members, which makes its carbon dioxide emissions higher than that of the GFRP pedestrian bridge. The construction stage of RC pedestrian bridge produces 390 $kgCO_2eq$ more than the GFRP one, accounting for carbon reduction of 45%. Similarly, a steel pedestrian bridge in the construction stage produces up to 646 $kgCO_2eq$ more than the GFRP pedestrian bridge yielding to 57% carbon reduction.

The largest carbon reduction benefit of the GFRP pedestrian bridge compared with an RC pedestrian bridge occurs at the transportation stage, then the construction stage, and lastly the production stage. The largest carbon reduction benefit of the GFRP pedestrian deck compared to a steel one occurs at the construction stage, then the transportation stage, and lastly the production stage. The carbon reduction of the GFRP pedestrian bridge compared with that of RC and steel pedestrian bridges are shown in *Table 5*. *Figure 12* is the comparison chart of the three different bridge types of carbon dioxide emissions.

Table 5. Comparison of carbon reduction benefits for the different materials and stages

Bridge type		GFRP bridge	RC bridge		Steel bridge	
Basic data	Length	8 *m*	8 *m*		8 *m*	
	Span	7.5 *m*	7.5 *m*		7.5 *m*	
	Width	1.5 *m*	2.14 *m*		1.5 *m*	
	Volume	714,314 cm^3	13,457,816 cm^3		391,704 cm^3	
	Weight	1,214 *kg*	33,540 *kg*		3,075 *kg*	
Evaluation ($kgCO_2eq$)	Production	5,334	8,583	Carbon reduction: 38%	6,048	Carbon reduction: 12%
	Transportation	64	787	Carbon reduction: 92%	90	Carbon reduction: 28%
	Construction	480	871	Carbon reduction: 45%	1,127	Carbon reduction: 57%
Total carbon footprint ($kgCO_2eq$)		5,879	10,241	Carbon reduction: 43%	7,265	Carbon reduction: 19%

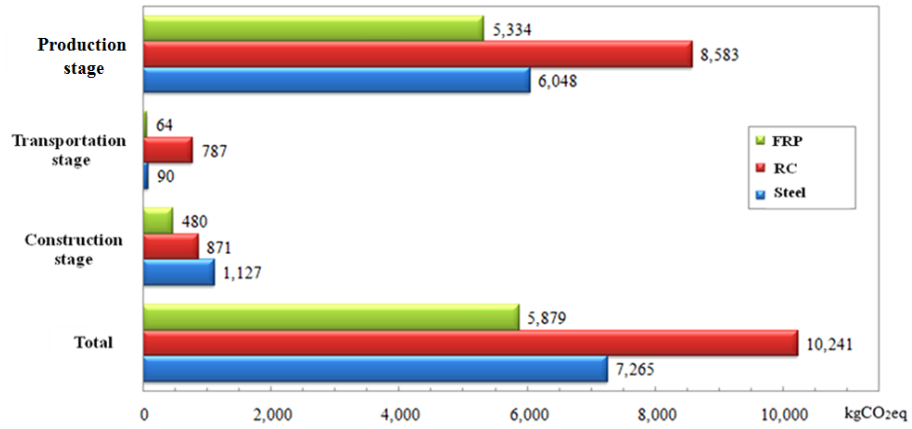

Figure 12. Comparison of the three different bridge types of carbon dioxide emissions

From *Table 5*, the carbon dioxide emissions for each stage shows that the GFRP pedestrian bridge has 43% reduction in carbon emissions over the RC pedestrian bridge, and 19% reduction in carbon emissions over a steel pedestrian bridge. Therefore, using GFRP material as an alternative material in constructing the pedestrian bridge has more carbon reduction benefits than traditional construction materials.

According to the document from the website of the Forestry Bureau (http://www.forest.gov.tw/ct.asp?xItem=59104 &ctNode=2577&mp=41), a tree will reduce carbon emission about 12 $kgCO_2eq$ per year. Comparing the GFRP pedestrian bridge with RC and steel pedestrian bridges, the reduced carbon emission of GFRP pedestrian bridge is equal to 363 trees for the RC bridge; and 115 trees for the steel bridge, respectively.

6. Conclusions

1. The safety factor of the GFRP pedestrian bridge is 20.4. The maximum allowable deflection from the design code, *L*/400 (1.87 *cm*), is 14.3%

larger than the GFRP pedestrian bridge in Tai-Jing National Park. Therefore, the GFRP pedestrian bridge can provide sufficient service performance and safety.

2. The weight of the superstructure of the GFRP pedestrian bridge is significantly less than the RC and steel pedestrian bridges. The lightweight nature of the bridge structural does not cause too much damage to the fragile ecosystems of the National Park.
3. Because of the GFRP material's lightweight, high-strength, and easy-to-assemble properties, the total carbon dioxide emission of the GFRP in various stages is significantly lower than traditional RC and steel pedestrian bridges, which makes GFRP material environmentally friendly.
4. A comparative analysis of the GFRP, RC and steel pedestrian bridges indicate that with the high-strength characteristics of GFRP composite material, under the same structural design conditions, a smaller cross section of the GFRP material can be used to achieve the same service performance. This also shows that the GFRP material has less carbon dioxide emissions in the production stage compared with the other two traditional construction materials.
5. In the transportation stage, although the transportation distance of the GFRP components was farther than that of the other two traditional construction materials, the lightweight property of GFRP components lowers their carbon emission and makes them easier to handle for assembly and installation.
6. There is no need for heavy construction machinery for GFRP pedestrian bridge, which in turn significantly reduces the carbon dioxide emission in the construction stage also.
7. Comparing the GFRP pedestrian bridge with RC and steel pedestrian bridges, the reduced carbon emission of GFRP pedestrian bridge is equal to 363 trees for RC bridge; and 115 trees for steel bridge, respectively.

REFERENCES

American Association of State Highway and Transportation Officials. (2008). *Guide specifications for design of FRP pedestrian bridges, 1st Edition.*

Composite Structure of Society of Civil Engineers Committee. (2011). *Guideline for design and construction of FRP pedestrian bridge*. (in Japanese)

Davalos, J.F., Salimet, H.A., *et al.* (1996). "Analysis and design of pultruded FRP shapes under bending", *Composites Part B: 27B*, 295-305.

Environmental Protection Administration of Taiwan. (2010). *Guidelines for carbon footprint calculation of products and services*.

Hammond, G., Jones, C. (2008). "Inventory of carbon and energy (ICE)", Version 1.6a, Sustainable Energy Research Team (SERT), Department of Mechanical Engineering, University of Bath, UK.

Hsu, C.W., Chen, A.H., *et al.* (2011). "Site selection for carbon dioxide geological storage using analytic network process", *Separation & Purification Technology*.

Hu, A.H., Lin, R.W., *et al.* (2011). "Carbon reduction assessment of a product service system-A case study of washing machines, eco-design", *The 7th Symposium on Environmentally Conscious Design and Inverse Manufacturing*, Kyoto, Japan.

Li, Y.F., Kan, S.T. (2011). "A study on the three-point bending test and mechanical behavior of the hybrid FRP beam", *2011 ICFMEIA*, Bali Island, Indonesia.

Li, Y.F., Hsu, T.H., *et al.* (2012). "Three-point bending test and finite-element analysis on FRP bridge deck", *The 9th International Conference on Urban Earthquake Engineering and 4ACEE*, paper ID 07- 091, p. 189, Japan, Tokyo.

Nakamura, S. *et al.* (2012). "Guidelines for Design and Construction of Fibre- Reinforced Polymer Footbridges in Japan", *Structural Engineering International*, 22(2), 250-253.

Nayomon, U., Kitayama, N. (2003). "Design, fabrication and erection of the pedestrian bridge in the road-park of Ikei-Tairagawa in Okinawa", *Engineering Review*, 36(2), 35-39.

Neto, A., Rovere, H. (2007). "Flexural stiffness characterization of fiber reinforced plastic (FRP) pultruded beams", *Composite Structures*, 81, 274-282.

Qiao, P., Davalos, J.F., *et al.* (2000). "A systematic analysis and design approach for single-span FRP deck/stringer bridges", *Composites Part B 31*, 593-609.

U.S. Department of Agriculture, Forest Service, Technology and Development Program. (2011). *A Guide to Fiber-Reinforced Polymer Trail Bridges*.

International review for spatial planning and sustainable development, Vol.1 No.4 (2013), 29-42
ISSN: 2187-3666 (online)
DOI: http://dx.doi.org/10.14246/irspsd.1.4_29

Copyright@SPSD Press from 2010, SPSD Press, Kanazawa

Using GIS and Hedonic in the modelling of spatial variation of housing price in Xiamen city

Yuan Li[1]*, Lang He[1], Wangtu Xu[1], Hui Wang[1], Zizhang He[2]
1 School of Architecture and Civil Engineering, Xiamen University
2 Xiamen Urban Planning & Design Institute
** Corresponding Author, Email: Yako79@gmail.com*
Received 16 December 2012; Accepted 5 July 2013

Key words: GIS, Housing Price, Spatial Variation, Hedonic, Xiamen City

Abstract: Valuing the built environment with the support of GIS and housing price model is an interesting topic because it connects the spatial thinking with economic concerns. In this paper, we chose the ordinary commercial housing in Xiamen City as our research targets, and the technology of GIS and Hedonic price model were used. Xiamen city is a typical coastal city, and from the research result, we found that the distribution of higher housing price was kept consistent with the coastal areas of Xiamen city. Besides, the average housing price of Xiamen inner-island (the old urban island area) was far higher than the outer-island. To reveal the degree of different spatial elements affecting housing price, we chose 21 variables (three types: location characteristic, structure characteristic and neighbourhood characteristic) and measured them in GIS platform. The Hedonic model showed that the main elements that influencing the price of commodity housings in Xiamen included Property Management Fee, Distance to Commercial Center, Distance to Hospital, Distance to Primary School, Near Village or Not, Near Green space or Not, Near kindergarten or Not. At the end of the paper, we provided three suggestions to balance the spatial variation of housing price in Xiamen City.

1. BACKGROUND

Housing, which is one of the most basic human needs, is a hot economic issue and social issues related to people's livelihood. Many factors influence the housing price and many researchers try to reveal the distribution rules on spatial variation in housing price. Some people (Xu, 1997; Jiang and Zhu, 2005; Meng, Zhang et al., 2005; Mei and Li, 2008) used GIS spatial interpolation method to get spatial distribution map and contour map of housing price. Some people (Luo, He et al., 2002) took Lanzhou as a case study and constructed the SD-GIS space-time simulation model to study the space-time distribution changes of residential price. Some (Montero and Larraz, 2009) considered that space in the real estate market is important and official averages do not take into account the spatial correlation of housing price. They proposed the Kriging mean method to estimate mean housing price. Some (Fik, Ling et al., 2003) hold the view that absolute location must be viewed as interacting with other determinants of housing value. They presented an interactive variables approach and tested its ability to explain price variation in an urban residential housing market. Some (Zhang, Meng et al., 2004; Armstrong and Rodríguez, 2006) established the Hedonic price method, studied the relationships between different traffic convenient degree

and house price. Some (Wang, Zheng et al., 2007) constructed Hedonic Model and analysed the degrees how urban public service accessibility influences housing price. Some (Cohen and Coughlin, 2008) revealed the relationship between airport noise level and real estate value. Some (Sedgley, Williams et al., 2008) detected how public school quality influence real estate markets in Howard County, Maryland. Some (Visser, Frank et al., 2008) used Hedonic price modelling to derive different models of property price from which the contribution of the characteristics of the residential environment were estimated. It was demonstrated that an important factor was the accessibility to employment opportunities. Some (Cho, Kim et al., 2009; Cho, Kim et al., 2012) took Knoxville, TN as an example , and focused on the relationship between neighbourhood environment and housing price. They suggested that vacant land should be reasoning to promote its value when the housing price around it rises.

However, from the literature review, we found that geography scholars mainly focused on spatial analysis and less quantitative description about causes. Meanwhile, real estate and city economics researchers mainly focused on the application of Hedonic method to study the external environment influence in housing price (Liu, Yang et al., 2010). In this paper, combined with the technology of GIS and Hedonic model, we systematically analyzed housing price spatial distribution characteristics and influencing factors in Xiamen. We hope that our research and results could provide decision support for urban planning and real estate development, especially in the city which located in the coastal area like Xiamen City.

2. STUDY AREA

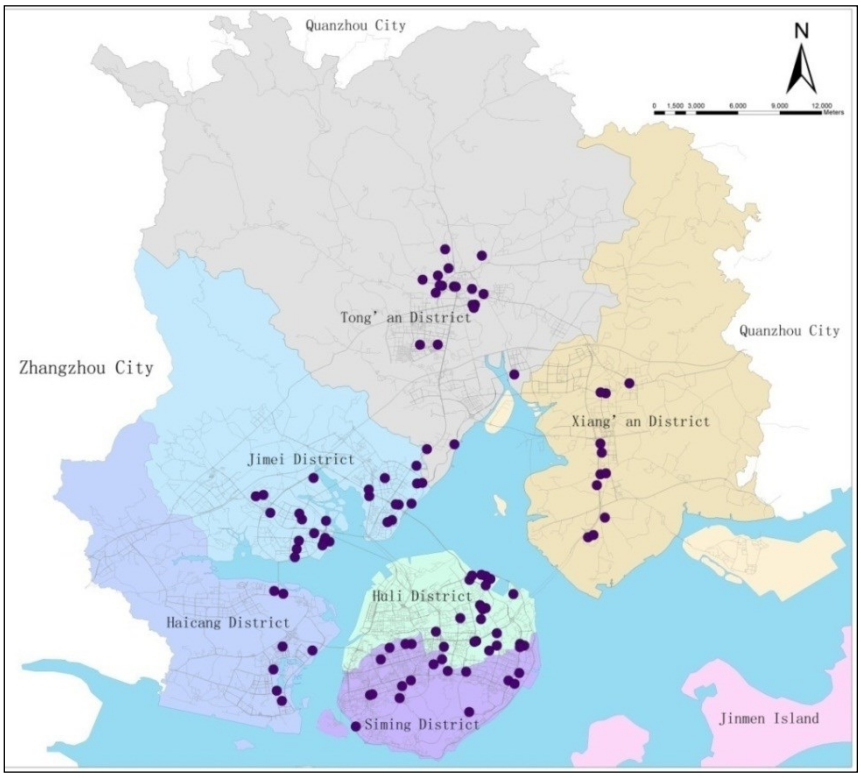

Figure 1. Study Area and the sample data (Xiamen City)

As one of the sub-provincial cities in Fujian Province (one of five municipalities directly under the central government and one of the first batch of five special economic zones in China), Xiamen owns several awards, including 'the United Nations living award', 'international garden city', 'national civilized city', 'national garden city', 'national the most liveable city', and many other honors. Taking built up area of Xiamen as the research scope, which includes Simon District, Huli District and most areas of Haicang District, Jimei District, Tong'an District and Xiang'an District. The administrative divisions of Xiamen city and sample distribution are shown in *Figure 1*.

The sample data is mainly from SouFun real estate website (http://www.soufun.cn/) and real estate advertising on newspapers. We collected 106 housing samples with integrated information. Besides, we used the basic GIS data from the government to establish a GIS database of Xiamen.

3. METHOD

3.1 Technical route

Combined with the GIS spatial analysis technology, we calculated the 21 variables for the three kinds of factors which describe the location characteristic, structure characteristic and neighbourhood characteristic. Using the SPSS software to perform regression analysis, we established an effective Hedonic price model to analyze the degree that characteristics influence the housing price. The technical route is shown as *Figure 2*.

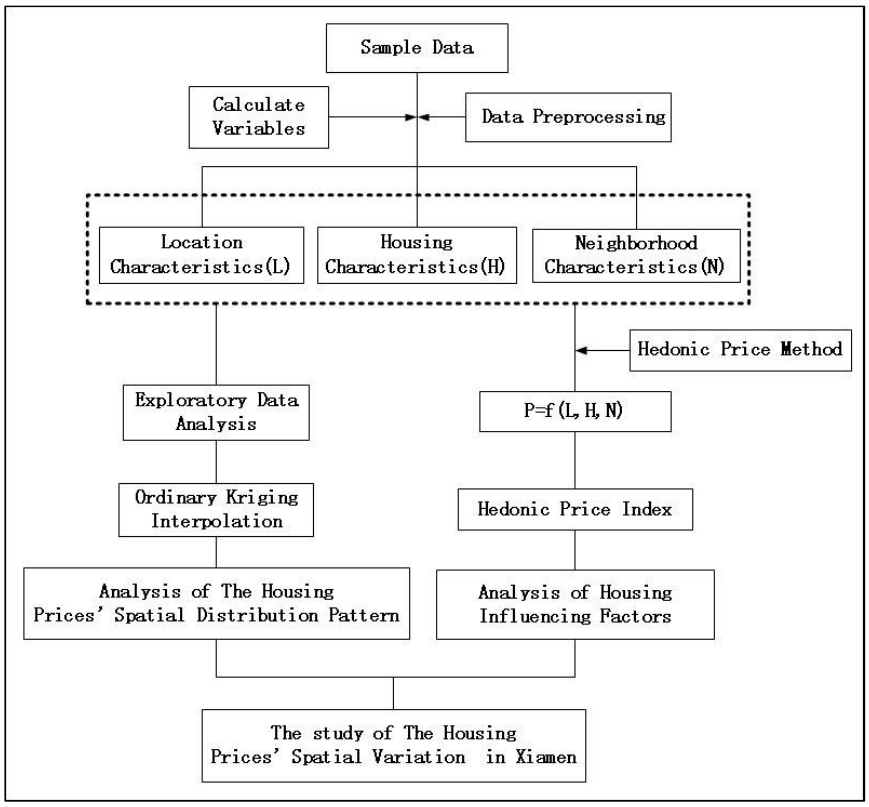

Figure 2. Technical route

3.2 Spatial Autocorrelation Analysis

Spatial autocorrelation analysis was used to test whether the property values in the adjacent space had a significant correlation. High correlation represented that the aggregation of space phenomena exists. Moran's index was commonly used to assess the spatial correlation and its value between -1 and 1. If 1>0, it was positively related to spatial entities showing aggregate distribution. If 1<0, it was negatively related to the spatial entity showing discrete distribution. If 1=0, it was unrelated and spatial entities were randomly distributed. The higher the value, the greater the spatial distribution of the correlation is. Moran's I formula is as *Formula (1):*

$$I = \frac{\mathrm{N}}{\sum_{\mathrm{i}=1}^{\mathrm{N}}\sum_{\mathrm{j}=1}^{\mathrm{N}} \mathrm{W}(\mathrm{i},\ \mathrm{j})} \times \frac{\sum_{i=1}^{\mathrm{N}}\sum_{j=1}^{\mathrm{N}} W(\mathrm{i},\ \mathrm{j})(\mathrm{X_i} - \bar{X})(\mathrm{X_j} - \bar{X})}{\sum_{i=1}^{\mathrm{N}} (\mathrm{X_i} - \bar{X})^2} \qquad (1)$$

In which N represents sample size that participate in analysis, $\mathrm{X_i}$ and $\mathrm{X_j}$ represents the observation at location i and j, and the observation is transaction average price. $\omega(i, j)$ represents the space distance weight, and it can be constructed by the adjacency rule and distance rules.

3.3 Kriging Interpolation

The Kriging method, also known as the spatial local interpolation method, was based on spatial autocorrelation. This kind of method used the structure of semi variable function to create unbiased optimal estimated regional variable values within a limited area. If the results of the variogram and structural analysis showed that the regional variable existed, researchers could take advantage of the method to interpolate or extrapolate the data, and otherwise it was not feasible. The Kriging method will take not only distance when interpolating data, but also the spatial distribution of the known samples and the orientation relationship between known sample's and unknown samples by variogram and structure analysis. The mathematical expression was shown as *Formula (2)*.

$$\mathrm{Z}(\chi_0) = \sum_{i=1}^{n} \omega_i \mathrm{Z}(\chi_i) \qquad (2)$$

In which $\mathrm{Z}(\chi_0)$ represents the values of unknown sample, $\mathrm{Z}(\chi_i)$ represents the values of known sample around unknown sample, ω_i represents the weights of the i known sample to unknown sample, and n represents the number of known sample.

3.4 Hedonic Price Method

Hedonic price method, also known as utility valuation method, was used in this paper. Usually, factors affecting the housing price were divided into

three categories: location (L), structure (S) and neighbourhood (N). The price could be formulated as *Formula (3)*:

$$P = f\left(L, S, N\right) \quad (3)$$

A Hedonic price model often adopts following three basic function forms in the empirical research.

1) Linear model

$$P = a_0 + \sum a_i c_i + \varepsilon \quad (4)$$

As shown in *Formula (4),* in which P represents the average residential price, a_0 is constant, c_i represents characteristic variable of order i, a_i is the characteristic price of variable i and ε is error.

2) Logarithmic linear model

$$InP = a_0 + \sum Ina_i c_i + \sum a_j c_j + \varepsilon \quad (5)$$

As shown in *Formula (5), i*ndependent and dependent variables adopt a logarithmic form. In which c_i is Continuous variable, c_j is neighbourhood attributes which can't take the logarithm. It is 0-1 variable.

3) Semi logarithmic linear model

$$InP = a_0 + \sum a_i c_i + \varepsilon \quad (6)$$

As shown in *Formula (6),* dependent variables adopt logarithmic form while the independent variable adopts a linear form.

4. ANALYSIS

4.1 Spatial Distribution Characteristics

We used the ArcGIS Geostatistics function to evaluate the spatial distribution of housing price in Xiamen. Figure 3 showed that the housing price was higher in the southern part of the island than the northern. Both east and west were lower than the middle and the curve present inverted "U". The housing price at Xiamen showed a very different non-linear distribution characteristic.

With ordinary Kriging interpolation method, we performed spatial interpolation analysis of sample data. Spatial distribution of ordinary housing price in Xiamen is shown as Figure 4.

The housing price in Xiamen city generally showed a strong single-center distribution pattern. The price in island area was a gradient decreasing process from the edge of the island to the inside area. The housing price of outside area was much lower than Xiamen Island. The highest price was around Zhongshan Road area. This area was the earliest commercial center in Xiamen city, where was a place close to the Gulangyu scenic zone and people gathered there in a long history.

Besides, it formed a housing price sub-center around Yuandang lake and train station. Administrative Centre and external traffic hub were located in these two areas where transport was convenient, scenery was beautiful and public service configuration was complete. In the outside island region, both Haicang District and Jimei District had a relatively higher level housing price than Tong'an District and Xiang'an District.

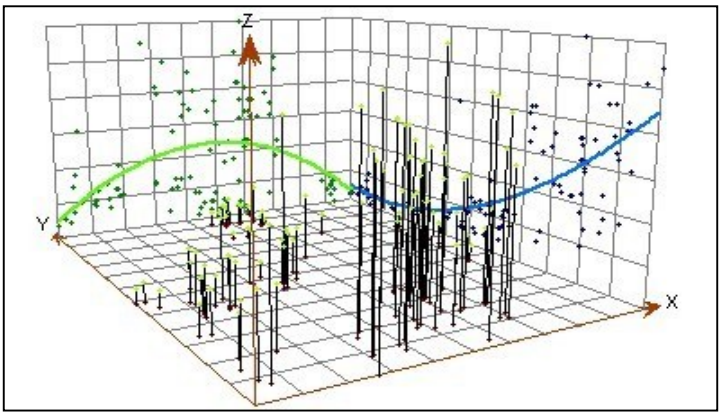

Figure 3. Trend surface of commodity housing price in main urban areas of Xiamen

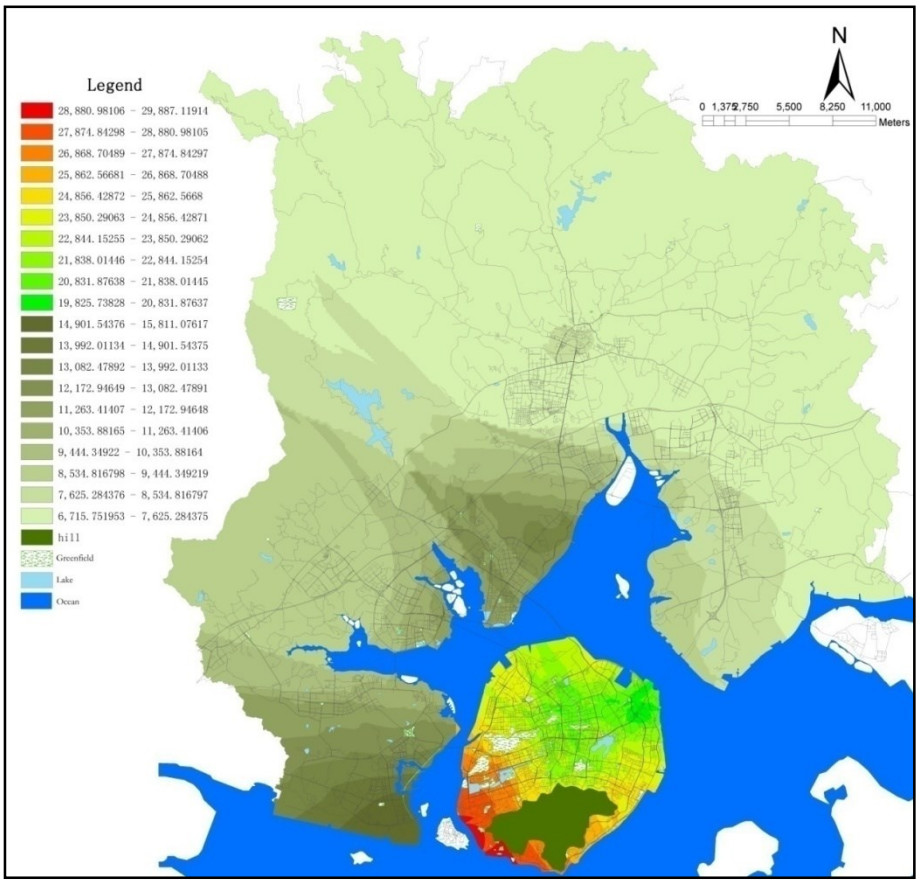

Figure 4. Spatial distribution of commodity housing price in main urban areas of Xiamen

4.2 Spatial Autocorrelation

According to the *Formula 1*, we used ArcGIS Spatial autocorrelation tool to calculate the Moran's I index of these 106 samples. The Moran's I index was 0.30 and the Z score was 16.34, which indicates that the housing price were clustered, rather than dispersed.

Using ArcGIS cluster and outlier analysis tool, we calculate the Local Moran's I index of housing price in Xiamen. The results were divided into 4 types, as shown in *Figure 5*. The red sample point indicates the price both this sample point and around it was higher than the average price of all

values. It's called local high value aggregation (high-high). There were 32 this kind of housing and they were all located in Xiamen Island where infrastructure was complete and the commercial environment was prosperous. The blue sample point indicated that the price of the sample point and around was lower than the average price of all values. It's called local low value aggregation (low-low). There were 29 this kind of sample and they all located in outside in Xiang'an District, Tong'an District and Jimei District. There was only one purple point and located in the junction area between JImei District and Tong'an District. It represented price to this point is higher than the average price of all values, but the housing price around was lower than the average price. It's called local high heterogeneous (high-low).

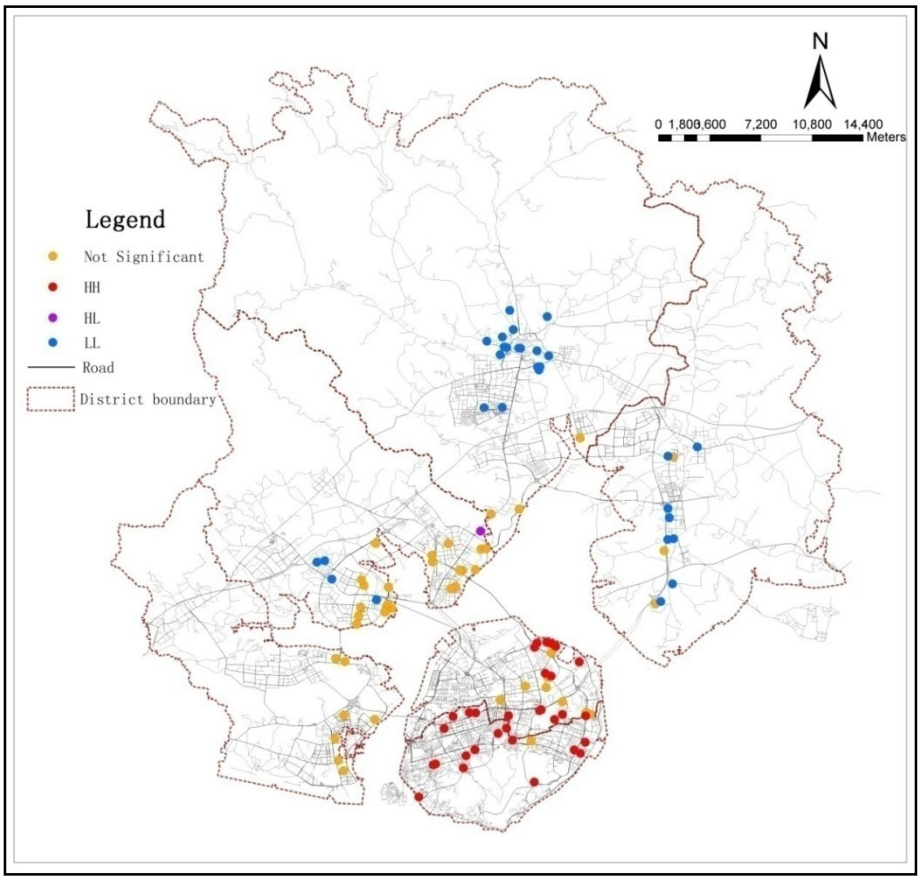

Figure 5. LISA of commodity housing price in main urban areas of Xiamen

4.3 Influencing Factors

Table 1. Characteristic variables of houses and their meanings

Category	Characteristic variable	Description and measurement of variable
Location	NextToOcean (X_1)	The closest distance from the ocean（m）
	NextToCC (X_2)	The closest distance from the commercial center（m）
	NextToKPSchool(X_3)	The closest distance from the key primary school（m）
	NextToKSSchool (X_4)	The closest distance from the key secondary school (m)
	NextToAC (X_5)	The closest distance from the administrative

		centre (m)
	NextToHospital (X_6)	The closest distance from the hospital (m)
Surrounding	PublicTransportservice (X_7)	Bus line numbers within 500m
environment	PShoolService (X_8)	If there is a primary school within 800m (0 or 1)
	SSchoolService (X_9)	If there is a secondary school within 1000m (0 or 1)
	KGService (X_{10})	If there is a kindergarten within 1000m (0 or 1)
	GreenFieldEffect (X_{11})	If there is green field within 500m (0 or 1)
	RailwayEffect (X_{12})	If in the 500m buffer area of railway (0 or 1)
	BankService (X_{13})	If there is a bank within 500m (0 or 1)
	VillageEffect (X_{14})	If there is a village within 500m (0 or 1)
Housing	BuildingArea (X_{15})	Building area (m^2)
	FloorArea (X_{16})	Floor area（m^2）
	Parking (X_{17})	Parking space
	Households (X_{18})	Households
	GreenRate (X_{19})	Green ratio (%)
	FAR (X_{20})	Plot ratio
	PropertyManagementFee (X_{21})	Property management fee（Yuan/month· m^2）

We selected 21 variables for our study. The variables were selected on the base of literature review and the availability of data. We classified the variables into three types: location characteristic, structure characteristic and neighbourhood characteristic. The characteristic variables are shown as in *Table 1*.

4.4 Hedonic Modelling

The standard method for estimating Hedonic price function was parameter method. First, we determined the functional form. Then, we needed to select the appropriate estimation method. Last, we needed to fit the sample data. In order to facilitate the estimation of parameters and interpretation, we made the hypothesis that the relationship between price characteristics was linear. Many researches adopt standard simple functions, such as a linear model, semi logarithmic model and logarithmic model, etc. The reason for selecting these function form was that the traditional least square estimation methods was convenient to statistical inference and hypothesis testing. In this paper, we estimated the housing characteristic price or marginal price through the model, then took the corresponding market analysis.

In Economic theory, there were no explicit rules to specify which function forms and feature variables Hedonic adopted for Hedonic housing modelling. Thus, this study compared the three kinds of functional forms in order to select a suitable model. Meanwhile, we monitored the co-linearity between variables by variance inflation factor (VIF).

Table 2 showed the parameter comparison of three functions. Linear model multiple correlation coefficient R was 0.901. It demonstrated that the fitting precision of linear model was better than the other two. Thus, we choose linear model to study the relationships between housing price and housing characteristics. According to the partial regression coefficient in the regression equation, we removed the factors that significant level larger than

10%. Combined with variance inflation factor (VIF) inspection, we weeded out the multicollinearity factors. Finally, there were 7 variables selected in the model. After running the regression analysis, the results were as shown in the *Table 3*.

Table 2. Comparison of three functions

Function type	R	R^2	Adjusted R^2
Linear model	0.901	0.812	0.800
Log-linear model	0.897	0.805	0.790
Semi-logarithmic model	0.874	0.764	0.754

Table 3. Regression coefficient analysis

	Non-standardized coefficient		Standardized coefficient			
Variable	B	Std Error	Beta	t	Sig.	VIF
Constant	5274.659	1446.784		3.646	.000	
PropertyManagementFee (X21)	4880.947	445.076	.613	10.967	.000	1.270
NextToCC (X2)	-.602	.153	-.218	-3.939	.000	1.247
NextToHospital (X6)	1.190	.387	.197	3.071	.003	1.675
NextToKPSchool (X3)	-.271	.127	-.123	-2.139	.035	1.354
VillageEffect (X14)	-2501.633	968.019	-.139	-2.584	.011	1.173
GreenFieldEffect (X11)	2974.278	1024.754	.163	2.902	.005	1.289
KGService (X10)	2572.500	1004.815	.137	2.560	.012	1.159

5. RESULTS

The regression coefficients for 7 characteristic variables of the linear model could be obtained by regression analysis. We calculated the housing Hedonic price model of Xiamen, as shown in *Formula (7)*:

$$Price=5274.659-0.602X_2-0.271X_3+1.19X_6+2572.5X_{10}+2974.278X_{11}-2501.633\ X_{14}+4880.947\ X_{21} \quad (7)$$

According to the results of regression analysis, we could find the main elements that influence the price of commodity housings in Xiamen: PropertyManagementFee (X_{21}), NextToCC (X_2), NextToHospital (X_6), NextToKPSchool (X_3), VillageEffect (X_{14}), GreenFieldEffect (X_{11}), KGService (X_{10}).

1) Proximity of the commercial centers (X2)

Generally speaking, commercial centers were the most active areas of a city as they provided various urban services and consumption choices for urban residents, which made it very convenient for people to live. Theoretically, the housing price in the surrounding area was relatively higher. It could be seen from the Hedonic price model that the variable coefficient of the distance to commercial centers was -0.602, suggesting that the distance from housing to business centers was inversely proportional to the housing price. With the distance between dwellings and business centers expanding, the residential price would fall. More specifically, every 1

kilometre of the increase in distance would cause 602 RMB (Yuan) loss in sale price.

2) Proximity of the hospitals (X6)

With the improvement of living standards, people paid more attention to medical and health care than before. As an important kind of public service, medical care provided protection for the life and health of the residents. "Time is life", the distances between dwellings and hospitals measured the residents' medical convenience. However, the coefficient of the model doesn't reflect the relationship that the houses price increases among with the distance increasing. The most reason is the models don't differentiate the needs of health care service between different age groups. The young people are strong and seldom go to the hospital. They usually will never take hospital into account even reject live close to hospital. Meanwhile the elderly people are more often go to the hospital. Considering the access of the data, the Hedonic model didn't specially research the age structure of families then ignored the elderly's preference close to hospital. In the Hedonic price model, the variable coefficient of hospitalization was 1.19, and it meant that the sale price would increase 1,190 RMB as the distance to hospitals increase 1 kilometer.

3) Proximity of the key primary schools (X3)

Education was the foundation of the nation, which was related to the quality of people and long-term development of the country. As the high-quality education resources were limited and unevenly distributed, many parents in China rent or even bought houses near key schools in order to offer their children with better education. As can be seen from the above Hedonic price model, the key primary schools had a positive effect on housing price and the sale price would decrease 1,190 RMB per kilometer as the distance to provincial-demonstrated primary schools increased.

4) Near village or not (X14)

With the increasing development of Chinese economy, the process of urbanization was becoming faster and faster. Urban construction and urban area expanded to the outlying regions, which made "villages surrounded by cities" become the most common phenomenon. The area that had not been urbanized could be found in the urban area, and this was called "village in the city". Cities were often close to rural settlements in the outreach process. The rural lands possessed features such as a high building density, a low greening rate, narrow and hindered streets, poor sanitation and so on because of land property restrictions and lack of reasonable and effective planning. Urban infrastructure and public service facility could not reach the whole city, so the development of urbanized area close to villages was kind of limited. As can be seen from the above Hedonic price model, villages had a negative effect on residential lands' externality. The average price of the premises near the village was 2,501.633 RMB lower than the ones far away from the village.

5) Near Greenland or not (X11)

As the living standard improves and awareness of environmental protection enhances, residents were more willing to purchase houses with comfortable environment. Being the open space of a city, public green lands possessed functions like landscape, airing and leisure. They were provided with social, economic and ecological value, and made the comfortable living and working environment accessible to residents. It could be concluded from the Hedonic price model that public green lands had a positive effect on urban residential lands' externality. The average price of the housings close

to greenbelts was 2,974.278 RMB higher than the ones far away from the green space.

6) Near kindergartens or not (X10)

It was not suitable for children to attend school through a long trip as they are at such a young age. On one hand, the overlong distance to kindergarten may cause safety problems. On the other hand, it would aggravate the parents' burden in picking up their children. As an important kind of neighborhood service, the kindergartens were supposed to be arranged near residential districts because of the object restrictions they served. In the Hedonic price model, the variable coefficient of kindergarten was 2,572.5, suggesting that the average price of housings near kindergartens was 2,572.5 RMB higher than that of housings far away from kindergartens.

7) Property management level (X21)

Property cost was a symbol of property management level. Decent property management indicated high-quality living conditions. As can be seen from the regression coefficients of characteristic variables, the property management level had a great influence on premises price. Housing prices would increase 4,880.947 RMB as long as the property cost increased 1 RMB.

Other variables, such as building area, household number, parking digits, volume rate, greening rate and so on, had little influence on housing price. It meant that the scale of premises can hardly affect people's consuming choice, while the parking digits, volume rate, greening rate, etc. were prescribed in urban controlling detailed planning and could meet people's needs of living.

6. DISCUSSION

1) Single-central city polarization development

Since the reform and opening up 30 years ago, the construction of Xiamen island had been highly concentrated, tended to saturation, presented as a typical single-central spatial structure (He, Qiu et al., 2007). Dense population, traffic congestion, landscape degradation, overtop property price had become a common problem on the main island, and urban construction or supporting facilities outside main islands had large lagged behind. The proportion of area between the main island and the outside was 1:11, and the proportion of population density was 11:1. 65% of the jobs distribute in the main island, and large cultural，educational and body health facilities, port airports，railway stations and the important traffic facilities were almost located in the main island. Polarization effect of the island was very obvious.

In recent years, some sea-crossing passages (such as JiMei Bridge, Xiang'An tunnels) have built. The infrastructures, for example, the port and the new railway station, have begun to locate outside the island. The construction of these functional facilities expands the city scale, however, the corresponding public facilities fail to timely follow-up and the city has not formed the strong anti-magnetic function. As a result, the broadening function of the outer island strengthens the single central polarization effect through the "diffusion - echo" effect, and the single-central structure is difficult to break at present. Single-central city structure decides Xiamen housing price on the spatial distribution pattern of a single center.

2) Unbalanced allocation of public facilities

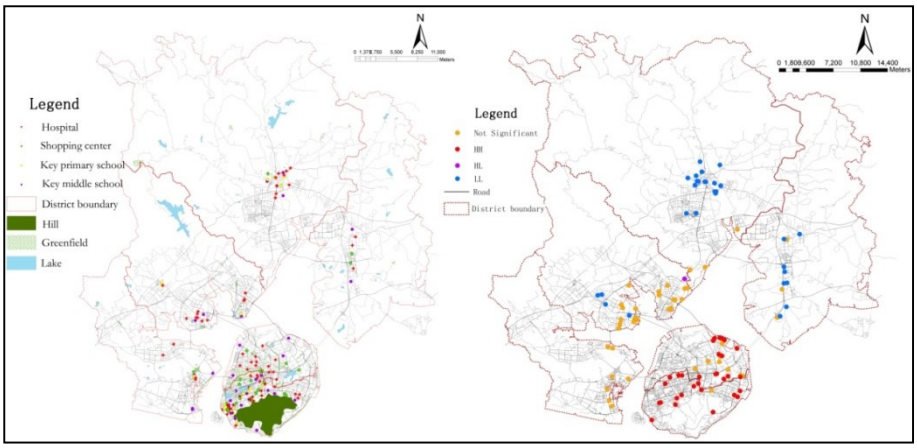

Figure 6. Compare of public service and housing price' LISA

Some researchers (Basu and Thibodeau, 1998) thought that housing price had spatial correlation for two reasons. One was that neighbouring areas tended to the same sequence development, resulting in adjacent area had the similar structural characteristics, such as residential size, building age, internal and external design style, etc.. Another reason was the adjoining property of enjoying the same convenience degree of public service facilities. Good accessibility of public service facilities was the important premise ensuring the residents' quality of life (Wang, Zheng et al., 2007). Although single-central polarization would bring a lot of problems, such as traffic congestion, environmental degradation, but high quality public service facilities owned much stronger appealing, which made people unconsciously live around the centre of the city. Consequently, these would lead to high housing price in the core area. As shown in *Figure 6*, the island highly concentrated the public service facilities, and the housing price was also high in the island area.

For a long time, Xiamen citizens had a traditional thought —"prefer a bed in the island, not a room outside the island ". In order to change this situation, we must improve the quality of new shopping, transportation, health care, education and other supporting facilities outside the island.

3) Geographical spatial partition

The gulf made the Xiamen city separated, and caused the urban spatial structure discontinuity. Due to the gulf division, the links between outside areas and the main island are bridges and tunnels. As shown in *Table 4*, the direct link between HaiCang, JiMei and Main Island was earlier (Year 1999 and Year 2008) through Haichang Bridge and Jimei Bridge. The direct link between Xiang'an and the main island is relatively late, and there is no direct link between Tong'an and the main island.

Table 4. The General situation of traffic projects connecting Xiamen Island and outside

Traffic project	Traffic time	Designed traffic capacity	Connection area	Passing vehicles
Haicang Bridge	December 30, 1999	5 ten thousand pcu /Day	Huli-Haicang	Car
Xinglin Bridge	September 1, 2008	3.38 ten thousand pcu/day	Huli-Jimei	Car /train
Xiamen Bridge	December 19, 1991	2.5 ten thousand pcu/day	Huli-Jimei	car

Jimei Bridge	July 1, 2008	5.5 ten thousand pcu/day	Huli-Jimei	car
Xiang'an Tunnel	26 April, 2010	5.2 ten thousand pcu/day	Huli-Xiang'an	Car

4) Coastal landscape effect

It was obviously that coastline, shoreline resources owned special or extra value because of its beautiful scenery. For Xiamen city, because of its pleasant climate, clean environment, rich historical and cultural background, the value of coastal landscape effects are even greater. A large number of market demand made the real estate price in coastal area higher than other area in Xiamen city. More specifically, in the island, the housing price was decreasing from the coastal line to the inside island, however, in the outside island, the housing price was increased from the inside to the outside coastal area.

7. CONCLUSION

This article discussed the spatial distribution in housing price in Xiamen City. It revealed the different spatial pattern of Xiamen housing price and found that the location characteristic, neighborhood characteristic and building characteristics had significant influences in housing price. At the end of the paper, we provide three suggestions. One is to strengthen the rapid transportation construction of the main island and outside, to shorten the space and time distance of the city area, to enhance the different geographical location accessibility, to strengthen the residents travel convenience. The second is to be optimized allocation of public service resources in the city area, especially to strengthen the regional and high quality public service facility configuration outside the island. The last is to weaken the polarizing effect of the island, to relocate parts of the city functions such as foreign transportation, administrative office, entertainment, business and trade of the island.

ACKNOWLEGEMENT

This work was financially supported by the Natural Science Foundation (NO. 41071101), Fujian Natural Science Foundation (NO. 2010J05099) and Special Fund for Scientific Research in Colleges and Universities (NO. 2012121033).

REFERENCES

Armstrong, R. J. and Rodríguez, D. A. (2006). "An evaluation of the accessibility benefits of commuter rail in eastern massachusetts using spatial hedonic price functions", *Transportation,* 33(1), 21-43.

Basu, S. and Thibodeau, T. G. (1998). "Analysis of spatial autocorrelation in house prices", *The Journal of Real Estate Finance and Economics,* 17(1), 61-85.

Cho, S., Kim, J., et al. (2012). "Neighborhood spillover effects between rezoning and housing price", *The Annals of Regional Science,* 48(1), 301-319.

Cho, S. H., Kim, S. G., et al. (2009). "Spatially-varying effects of rezoning on housing price", *Review of Urban & Regional Development Studies,* 21(1), 72-91.

Cohen, J. P. and Coughlin, C. C. (2008). "Spatial hedonic models of airport noise, proximity, and housing prices", *Journal of Regional Science,* 48(5), 859-878.

Fik, T. J., Ling, D. C., et al. (2003). "Modeling spatial variation in housing prices: A variable interaction approach", *Real Estate Economics,* 31(4), 623-646.

He, Z. Z., Qiu , G. C., et al. (2007). "Research of xiamen urban morphology development based on space syntax analysis", *Huazhong Architecture,* 25(3), 106-108.

Jiang, F. and Zhu, D. L. (2005). "A gis-based study on spatial distribution of land prices, the case of residential land prices in beijing", *Economic Geography,* 25(2), 199-202.

Liu, D. H., Yang, Y. C., et al. (2010). "Study on the spatial distribution of housing price and its influencing factors in chengdu based on gis and hedonic model", *Journal of Anhui Agricultural Sciences,* 38(29), 16519-16523.

Luo, P., He, S. F., et al. (2002). "A case study of space-time simulation of lanzhou's urban housing prices using the sd-gis model", *JOURNAL-LANZHOU UNIVERSITY NATURAL SCIENCES,* 38(4), 125-130.

Mei, Z. X. and Li, X. (2008). "Spatial analysis of houses' price in dongguan based on esda and kriging techniques", *Economic Geography,* 28(5), 862-866.

Meng, B., Zhang, J. Q., et al. (2005). "Application of spatial analysis to the research of real estate:Taking beijing as a case", *Geographical Research,* 24(6), 956-964.

Montero, J. M. and Larraz, B. (2009). "Estimating housing prices: A proposal with spatially correlated data", *International Advances in Economic Research,* 16(1), 39-51.

Sedgley, N. H., Williams, N. A., et al. (2008). "The effect of educational test scores on house prices in a model with spatial dependence", *Journal of Housing Economics,* 17(2), 191-200.

Visser, P., Frank , V. D., et al. (2008). "Residential environment and spatial variation in house prices in the netherlands", *Tijdschrift voor economische en sociale geografie,* 99(3), 348-360.

Wang, S. T., Zheng, S. Q., et al. (2007). "Spatial accessibility of housing to public services and its impact on housing price: A case study of beijing's inner city", *Progress in Geography,* 26(6), 78-85+147-148.

Xu, X. H. (1997). "An analysis on the spatial distribution characters of commercial residence price in shanghai", *Economic Geography,* 17(1), 80-87.

Zhang, W. Z., Meng, B., et al. (2004). "Influence of traffic passages on housing spatial expansion and local residents' selection of housing location--a case study of beijing", *Scientia Geographica Sinica,* 24(1), 7-13.

International review for spatial planning and sustainable development, Vol.1 No.4 (2013), 43-49
ISSN: 2187-3666 (online)
DOI: http://dx.doi.org/10.14246/irspsd.1.4_43

Copyright@SPSD Press from 2010, SPSD Press, Kanazawa

Planning Review: Application of Vertical Greening for Landscape Beautification in Taipei

Chien-Yuan Lin[1*] and Yin-Ling Huang[1]
1 Graduate Institute of Building and Planning, National Taiwan University
** Corresponding Author, Email: cylin@ntu.edu.tw*
Received 3 Feberuary 2013; Accepted 31 July 2013

Keywords: Vertical Greening, Landscape, Construction Fences, Environmental Benefit

Abstract: For the improvement of city landscape, vertical greening by plantation is one of the effective approaches. In the past few years, vertical greening has gained significant progress in both technological development and practical application. Thanks to the 2010 Flora Expo, vertical greening has made significant contribution to the landscape beautification in Taipei. Among various applications, temporary greening of fences surrounding construction sites has developed a unique landscape for Taipei city. In this paper, potential environmental benefits and application experience of vertical greening in Taipei city will be reviewed and discussed.

1. INTRODUCTION

Vertical greening is sometimes called as three-dimensional afforestation, perpendicular greening, and greening wall, etc. In horticulture, it is also often called as vertical gardening (Perini, K., Ottelé, M., et al., 2011). Usually, vertical greening is applied on vertical surfaces such as wall surface, fence, bar fence, vertical column and flower frames. It is regarded as one of the effective ways in the development of green buildings and eco-cities. To achieve effects of heat insulation, greening and beautification, vertical greening can either be cling plants or pending plants in practical applications. Broadly speaking, any form of greening on vertical structures can be named as vertical greening. Vertical greening can not only be applied to beautify city landscape, but also to promote the development of sustainable environment (Maas, J., Verheij, R.A., et al., 2006). In recent years, vertical greening has achieved significant progress in both technology development and practical applications in Taiwan. In this paper, the application experience of vertical greening for the landscape beautification in Taipei city, particularly the beautification program of fences surrounding construction sites by vertical greening, will be reviewed and discussed.

2. APPLICATION OF VERTICAL GREENING IN CITY LANDSCAPE IMPROVEMENT

Despite the scale of space, city landscape provides people visual perception of a place on a particular time. However, “time” factor is often neglected in landscape planning and management (Bolan, R.S., 2009).

Because of the difference in temporal scope and individual experiences, a temporary scene unusually experienced by a visitor may be just a usual phenomenon for local people (Temel, R., 2006). For instances, a local cultural event provides temporary experience for tourists, it is the only once for the tourists' whole life, but the annual event is actually just a regularly seasonal landscape for local residents. To provide impressive visual experience for tourists, a city has to design and manage landscape from the viewpoint of tourists. Therefore, the application of vertical greening is regarded as an effective way to create unique landscape experience for tourists.

In a densely developed city such as Taipei, where population and buildings are concentrated in limited area, horizontal expansion of greening space is very difficult. The application of vertical greening has become relatively more flexible for practical uses because plants can be attached on either the wall surface of buildings or other vertical surfaces.

Table 1 shows that vertical greening can be applied in different ways according to variables in time (temporary or permanent) and space (Indoor or outdoor). For instance, the National Music Hall in Taipei has used vertical greening to decorate indoor space for ordinary use, while many other business buildings have widely applied vertical greening to beautify outdoor spaces for permanent outlook. Fences surrounding construction sites are examples of temporary application in outdoor space, while many cultural events use vertical greening to decorate venue for temporary visual effect. In this paper, we will focus on the temporary outdoor application of vertical greening on construction sites.

Table 1. Types of Vertical Greening Application

Time \ Place	Indoor	Outdoor
Permanent Use	Musician Hall Shopping Center	Business Building Government Building
Temporary Use	Special Event or Activity	Fence surrounding Construction site

In terms of location, construction sites can be grouped into two types, namely, roadway and building. Different applications of vertical greening bring different impacts on surrounding environments. While the roadway construction projects bring significant traffic and visual impacts on wide areas, building sites have generated social and visual impacts on neighbors within relatively limited area. In either case, the application of vertical greening has resulted significant effects on the improvement of visual impacts. Traditionally, due to the nature of temporary use, ugly fences of various construction sites are taken for granted. Because of the application of vertical greening technology, better landscape with greening can be created now.

To develop an eco-city, any approach that which has potential contribution to environmental sustainability should be attempted in modern city planning and management. As a matter of fact, we have witnessed that vertical greening technology has become widely applied by more and more architects in the design of green buildings and landscapes. In most cases, they are applied to conserve energy consumption by insulating building

walls from solar heat. In Taiwan, it has been applied on the walls of various business buildings and government buildings. It not only beautifies the building outlook, but also establish brilliant and unique image for the building. The left of *Figure 1* shows the first outdoor application of vertical greening on private business building in Taichung City that which has become the attractiveness of the bookstore located in that building. The right of *Figure 1* shows the application of vertical greening on campus entrances of National Taipei University of Technology. It was once reported by TV Discovery program globally. In fact, thanks to its strategic location, it has well demonstrated the visual effects in landscape beautification and environmental design education.

Figure 1. Outdoor Application of Vertical Greening on Business Building (left) and UTUT Campus (right)

3. VERTICAL GREENING OF CONSTRUCTION FENCES IN TAIPEI

Due to the visual beautification effect, vertical greening technology is often used for temporary occasions such as event decoration and landscape beautification. Among various recent applications, the compulsory vertical greening of fences outside construction sites along main roads in Taipei is the most significant case. Traditionally, fences surrounding construction sites are made of irons for the sake of security to prevent outside interruption. Visual impact on city landscape has never been considered in the process of design and installation. To prepare for the 2010 Flora Expo in Taipei, all kinds of vertical greening were designed and established in many places from 2009 in order to establish unique image of 2010 Flora Expo. Meanwhile, to take advantage of the big event, the Taipei City Government initiated the so-called “Taipei Beautiful Program” in 2009 to beautify the landscape of Taipei city, for at least during the time of Flora Expo. “Taipei Beautiful Program” was actually a composition of 8 action series and 3 integrated action series. Among those action series, Series 3 was aimed at the application of greening technology to beautify the city landscape. Therefore, the Department of Urban Development of Taipei City Government established a new rule for their management of construction sites. The rationale is that all new construction sites are responsible for the visual quality of city landscape and each construction site should make contribution to beautify their fences during construction period. For those construction sites along main streets (width > 10m), they should adopt vertical greening for at least half of the fence surfaces. For those

construction sites along small roadways (width < 10m) should be painted or attached with approved posters. *Figure 2* are examples of vertical greening applications on construction site fences in Taipei.

Figure 2. Example of vertical greening on construction fences in Taipei

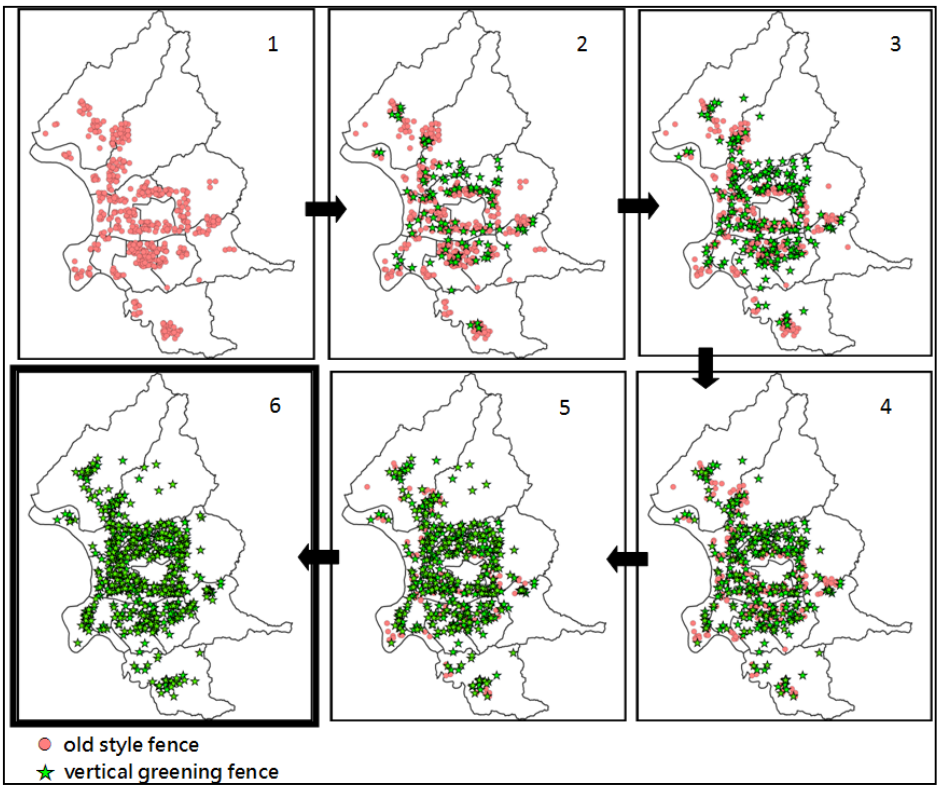

Figure 3. Example of vertical greening on construction fences in Taipei
Note: Red circle stands for old construction sites with iron fence, green star stands for new construction site with vertical greening fence.

According to Taipei city government, about 250 construction permits are issued annually in average, and each construction site usually takes about 4 years to complete. By and large, about 1000 construction sites distributed within Taipei city although their locations are partly varied every year because of the closure of old ones and the opening of new ones. The compulsory vertical greening program of construction fences was initiated from 2009, every year about 250 new constructions were added with vertical greening fences, while another 250 old construction sites with traditional iron fences were completed and closed in the city. By the end of 2012,

almost all construction sites along main streets in Taipei city are decorated with vertical greening fences. Through such progressive changing process, the city landscape is gradually transformed and construction site with vertical greening fence has now become a regular landscape, despite the fact that vertical greening fences are just temporary installations for each construction sites.

Figure 3 shows the temporal changing process of city landscape because of the vertical greening required for construction site fences in Taipei. In *Figure 3*, the red circle stands for old construction sites with iron fence, while the green star dot stands for new construction site with vertical greening fence. Because of the life cycle of 4 years for a construction site, it takes about four to six years to change the city landscape for permanent effects.

In order to encourage construction sites to design and adopt beautiful vertical greening fences, the Taipei City Government also conducted a competition program every year to recognize and award those sites with significant contribution to city beautification. The first competition was conducted in 2009, and the most recent competition was conducted in December of 2012. Every year, more than 50 construction sites registered for competition. *Figure 2* are examples of winners in 2012 vertical greening competition. Winners are very proud of their recognitions received, especially for those estate developments luxury houses. The success of the vertical greening competition is partly contributed by the cooperation of the Chamber of Real Estate Developers in Taipei city.

In recognition of the visual contribution of vertical greening, based on Taipei experience, more and more other cities in Taiwan adopt similar programs in their management of construction site fences.

4. ENVIRONMENTAL BENEFITS OF VERTICAL GREENING FENCES

Integration of vertical greening technology into construction industry has become a trend of environmental management in Taiwan. A vertical wall covered by green plantation will not only beautify the landscape, but also improve air quality and energy conservation in cities. If vertical greening is properly installed and integrated with surrounding environments, it can generate environmental benefits in various ways. Based on the experience of Taipei city, benefits of vertical greening application on fences surrounding construction sites are summarized as follows:

A. Visual experience quality

In contrast to traditional beautification of fences by painting, vertical gardening offers the city an excellent opportunity to enjoy diversified plantation color and shapes for landscape beautification.

B. Environment impacts

When plantations of vertical greening are chosen according to local ecological environmental features and constraints, it can produce counter-effect to mitigate the impact of traffic emission and ash particles on air quality.

C. Horticultural education benefits

The application of vertical greening in construction fences offers opportunities for construction workers to cooperate and take care of environmental maintenance in order to keep plants alive.

D. Better social relationships

A good design of construction fence is not only helpful to city landscape, but also provides a friendly environment for pedestrians. *Figure 2* shows the vertical greening fence for a construction site in Neihu of Taipei that which not only provides comfortable space for pedestrians, but also keeps the raining water flowing toward inside of construction. In some cases, plants on construction fences are offered as gifts to neighbors for better community relationship.

E. Development of horticulture industry

The wide application of vertical greening has also stimulated the development of horticulture industry. Large quantity of flowers and plants are demanded and used by many construction sites. Meanwhile, demand of fence maintenance also creates another business opportunity for horticulture skills.

In summary, both living environment and life quality of people in the city are improved because of the aforementioned benefits. However, the Taipei experience also shows that a well-operated system for plant maintenance is critically needed. A poorly maintained plantation will be a disaster to the city landscape.

5. SUMMARY

For the development of low-carbon city, landscape greening by plantation is widely regarded as one of the effective approaches. The application of vertical greening technology for greening building and sustainable city development has thus become widely adopted globally. In this paper, we have demonstrated how vertical greening technology can be an effective approach for local cities to improve city landscape. The vertical greening fences adopted for construction sites not only make contribution to better environmental quality, but also establish a more beautiful landscape of Taipei city. In fact, more and more cities began to follow the practical applications in Taipei city. Horticulture industry for applications of vertical greening has grown up steadily in Taiwan.

In addition to the benefits for environmental air quality and visual landscape, the Taipei experience also demonstrated the benefits of better social relation and environmental education resulted from the vertical greening fence program. However, it should be noticed that vertical greening of construction fences can be a visual disaster to city image if plants on vertical fences are not properly cared. Maintenance and quality management of vertical greening is thus a critical task for constructors, especially in summer time under hot temperature. Another challenge for vertical greening of construction fences is the way of disposal after use. Hundreds and thousands of pots of plants are to be discarded when construction work completed. If they are not properly disposed, it will be a waste of plants and a disaster to the development of sustainable environment.

From the experience of construction fence management in Taipei, we have learned that progressive accumulation of temporary beautification on

different sites has made up a unique city landscape. It has demonstrated that the improvement of city landscape needs efforts in all possible ways, including temporary landscape, in order to create significant change. Looking into future, In order to gain more public support for vertical greening application, evaluation of significant economic benefits is needed. We need to actively promote green infrastructure systems to secure the funding to build and maintain green space systems (Benedict, M.A. and McMahon, E.T., 2003). To develop appropriate software to calculate all kinds of social benefits (Barbosa, O., Jamie, A., et al., 2007), methodologies for quantitative assessment of social benefits from the application of vertical greening is thus another important task for future research (Abkar, M., Kamal, M., et al., 2011).

REFERENCES

Abkar, M., Kamal, M., et al. (2011). "Determining the Visual Preference of Urban Landscapes", *Scientific Research and Essays*, 6(9), 1991-1997.

Barbosa, O., Jamie, A., et al. (2007). "Who Benefits From Access to Green Space? A Case Study from Sheffield, UK", *Landscape and Urban Planning*, 83, 187-195.

Benedict, M.A. and McMahon, E.T. (2003) "Green Infrastructure: Smart Conservation for the 21st Century", *Renewable Resource Journal*, 20 (3), 12-17.

Bolan, R.S. (2009). "Saving Time-Losing Ground", *Journal of Architectural and Planning Research*, 26(2), 136-144.

Maas, J., Verheij, R.A., et al. (2006). "Green space, Urbanity, and Health: How Strong is the Relation?", *Journal of Epidemiology and Community Health*, 60(5), 87-92.

Perini, K., Ottelé, M., et al. (2011). "Greening the Building Envelope, Façade Greening and Living Wall Systems", *Open Journal of Ecology*, 1(1), 1-8.

Temel, R. (2006). "The Temporary in the City", in Hadyn, F. and Temel, R. (eds.), *Temporary Urban Spaces: Concepts for the Use of City Spaces*, Birkhauser, Berlin, 55-62.

IRSPSD International

ISSN 2187-3666 (Online)

For investigation regarding the impact of planning policy on spatial planning implementation, International Community of Spatial Planning and Sustainable Development (SPSD) seeks to learn from researchers in an integrated multidisciplinary platform that reflects a variety of perspectives—such as economic development, social equality, and ecological protection—with a view to achieving a sustainable urban form.

This international journal attempts to provide insights into the achievement of a sustainable urban form, through spatial planning and implementation; here, we focus on planning experiences at the levels of local cities and some metropolitan areas in the wolrd, particularly in Asian countries. Submission are expected from multidisciplinary viewpoints encompassing land-use patterns, housing development, transportation, green design, and agricultural and ecological systems.

International Review for Spatial Planning and Sustainable Development
https://www.jstage.jst.go.jp/browse/irspsd
http://spsdpress.jimdo.com/volumes/
http://dspace.lib.kanazawa-u.ac.jp/dspace/bulletin/irspsd